Geophys. J. Int. (2000) **143,** 629–661

A re-assessment of focal depth distributions in southern Iran, the Tien Shan and northern India: do earthquakes really occur in the continental mantle?

A. Maggi, J. A. Jackson, K. Priestley and C. Baker

University of Cambridge, Department of Earth Sciences, Bullard Laboratories, Madingley Road, Cambridge, CB3 0EZ, *UK.*
E-mails: maggi@esc.cam.ac.uk; jackson@esc.cam.ac.uk; keith@esc.cam.ac.uk

Accepted 2000 May 30. Received 2000 May 16; in original form 1999 December 7

SUMMARY

We investigate the depth distribution of earthquakes within the continental lithosphere of southern Iran, the Tien Shan and northern India by using synthetic seismograms to analyse *P* and *SH* body waveforms. In the Zagros mountains of southern Iran, earthquakes are apparently restricted to the upper crust (depths of <20 km), whereas in the Tien Shan and northern India they occur throughout the thickness of the continental crust, to depths of $\sim$40–45 km. We find no convincing evidence for earthquakes in the continental mantle of these regions, in spite of previous suggestions to the contrary, and question whether seismicity in the continental mantle is important in any part of the world. In some regions, such as Iran, the Aegean, Tibet and California, seismicity is virtually restricted to the upper continental crust, whereas in others, including parts of East Africa, the Tien Shan and northern India, the lower crust is also seismically active, although usually less so than the upper crust. Such variations cannot reliably be demonstrated from published catalogue or bulletin locations, even from ones in which depth resolution is generally improved. In contrast to the oceanic mantle lithosphere, in which earthquakes certainly occur, the continental mantle lithosphere is, we suggest, virtually aseismic and may not be significantly stronger than the lower continental crust. These variations in continental seismogenic thickness are broadly correlated with variations in effective elastic thickness, suggesting that the strength of the continental lithosphere resides in the crust, and require some modification to prevalent views of lithosphere rheology.

Key words: continental mantle lithosphere, earthquakes, lithosphere rheology.

1 INTRODUCTION

The distribution of earthquake focal depths within the lithosphere is one of the most accessible indicators of its likely mechanical properties. In the continents, and away from obvious subduction zones, seismicity is usually concentrated in the upper 10–20 km of the crust and the lower crust is usually much less active or even completely aseismic (e.g. Chen & Molnar 1983; Chen 1988). These observations, combined with a clear correlation between the depth of the deepest oceanic intraplate earthquakes and the age of the oceanic lithosphere in which they occur (e.g. Wiens & Stein 1983), are usually taken to indicate that temperature is the dominant control on seismicity, with earthquakes restricted to regions of relatively low temperature (e.g. Brace & Byerlee 1970). Chen & Molnar (1983) estimated the limiting temperatures for earthquakes in crustal and mantle materials to be about 350 ± 100 °C and 700 ± 100 °C respectively, the different temperatures reflecting their contrasting compositions. Chen & Molnar (1983) and Chen (1988) also emphasized the occurrence of rare continental earthquakes close to probable Moho depths and perhaps in the uppermost continental mantle. These earthquakes were taken to indicate an important strength contrast between the lower crust and the mantle. The observations summarized above are largely responsible for a view of the continental lithosphere in which a lower crust of relatively low strength, where aseismic ductile deformation predominates, is sandwiched between relatively strong upper crustal and uppermost mantle seismogenic regions. This view has had an enormous influence on our views of continental tectonics.

This study re-examines the depth distribution of the seismicity in four regions: the Zagros and Makran of Iran, the Tien Shan of central Asia, and northern India. It was motivated by three developments.

(i) The first was the discovery that not all areas were as simple as the picture summarized earlier. In parts of the East African rift system, usually near or within Archaean shields, earthquakes occur throughout the thickness of the continental crust to depths of approximately 35 km, prompting a re-examination of the likely rheology of those regions (e.g. Nyblade & Langston 1995; Zhao *et al.* 1997; Foster & Jackson 1998). Earthquakes to depths of 30–40 km have also been found around the Shillong Plateau (Chen & Molnar 1990), near Lake Baikal in Siberia (Déverchère *et al.* 1991), and around the margins of the Caspian Sea (Priestley *et al.* 1994).

(ii) The second development was the relocation by Engdahl *et al.* (1998) of earthquakes in the International Seismological Centre (ISC) catalogue between 1964 and 1995 (subsequently updated to 1998) using an improved velocity model and also including the arrival times of additional phases, particularly teleseismic depth phases *pP*, *pwP* and *sP*, to supplement the direct *P* arrival times in the relocation procedure. In principle, these relocations (which we refer to as the EHB catalogue) should be better than the original ISC locations, and Engdahl *et al.* (1998) demonstrated that this is the case in several subduction zones, where improved depths give a sharper image of the descending slabs. The EHB catalogue shows a number of earthquakes deeper than 50 km in the Zagros, where previously none had been confirmed below 20 km, and, in the light of the Africa, Baikal and Caspian experiences, we wanted to see whether these were genuine.

(iii) A third recent development was the re-assessment of effective elastic thicknesses on the continents using gravity and topography by McKenzie & Fairhead (1997). Their general conclusion that the effective elastic thickness (T_e) on the continents is probably close to the thickness of the seismogenic crust (T_s) allows the simple interpretation that the strength of the lithosphere resides in that layer, although they were unable to estimate the depth to the top of any elastic layer. Since McKenzie & Fairhead's (1997) study, more information on T_e variations in Asia is now available (Maggi *et al.* 2000), and we wanted to see how these variations correlated with variations in T_s.

This study thus has two aims. One is to see whether the undoubted general improvement in locations shown by the EHB catalogue (Engdahl *et al.* 1998) is sufficiently good to reveal anomalies in the usual pattern of earthquake depth distribution on the continents. The second, and more important, is to see whether our rheological views of the continental lithosphere based on earthquake focal depths need modification in the light of the large amount of extra data now available since the original studies of 15–20 years ago.

We focus on four main regions: the Zagros and Makran of Iran, the Tien Shan, and northern India. The Zagros mountains form a linear intracontinental fold-and-thrust belt trending NW–SE between the Arabian shield and central Iran (Fig. 1). The belt is seismically very active, with frequent reverse faulting earthquakes of up to M_s7.0. Early studies used the presence of earthquakes deeper than 50 km in the ISC or USGS catalogues to postulate subduction of the continental Arabian shield beneath Iran in the Zagros (Nowroozi 1971; Bird *et al.* 1975), a view sometimes repeated more recently (e.g. Moores & Twiss 1995). However, neither local seismograph networks nor the modelling of teleseismic body waves from the larger earthquakes have found any focal depths deeper than 15–20 km (e.g. Jackson & Fitch 1981; Ni & Barazangi 1986; Baker *et al.* 1993). Moreover, in an earlier study Jackson (1980) showed that the apparently deep earthquakes were mostly poorly recorded by relatively few stations, which increases the trade-off between origin time and depth. Thus it appeared that there was no

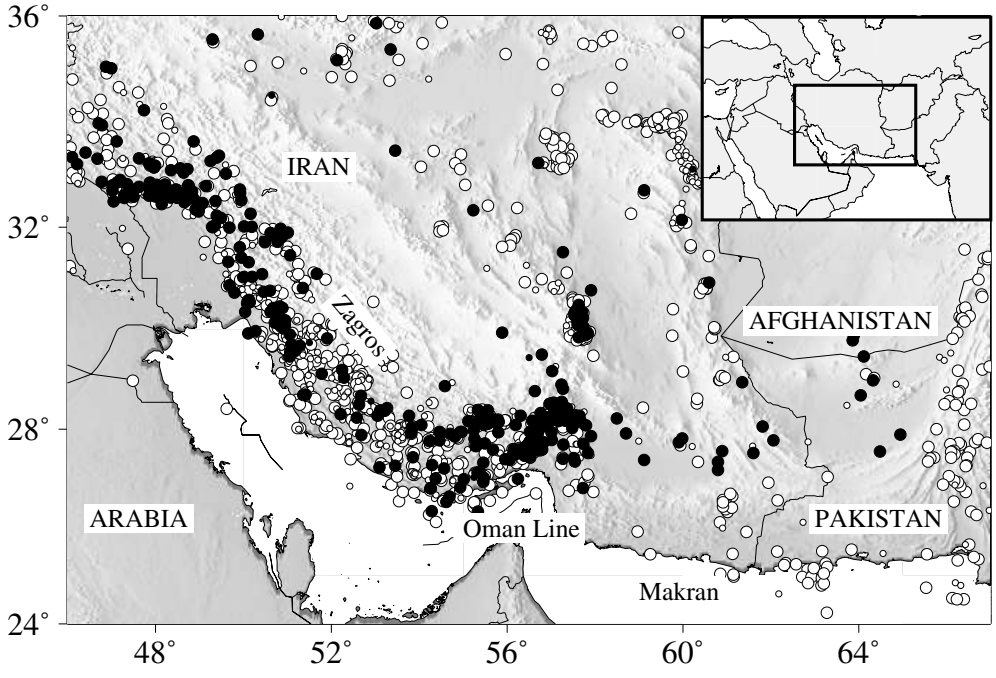

Figure 1. Seismicity in southern Iran from the Engdahl *et al.* (1998) catalogue (EHB) for 1964–1998. Events reported as shallower than 50 km are shown in white, while those reported at 50 km or deeper are shown in black. Large circles are those events whose depths were freely determined (flag DEQ) while small circles are events whose depth was fixed by the operator (flag FEQ; see text). The EHB catalogue is complete down to M_w5.2, although the magnitude range extends down to M_w4.5. The geographical location of the region is shown in the inset map.

evidence in the seismicity for subduction of continental crust, and shortening appeared to be accommodated by crustal thickening instead, with seismicity confined to the upper 20 km. However, more recently, the EHB catalogue and both the Harvard and USGS Centroid Moment Tensor (CMT) catalogues have reported depths as great as 80 km, even for quite large earthquakes whose waveforms can be studied in detail (Fig. 1 and Table 1). These depths, if correct, would require a re-assessment of our current views of the active tectonics.

At its southeastern end, the continent–continent collision zone in the Zagros merges along strike with the subduction of the Arabian Sea floor beneath the Makran coast. The change from continent to ocean occurs near 57°E in a region of complicated structure known as the Oman Line (Fig. 1). The Makran subduction zone is known to produce earthquakes to depths of approximately 200 km (Jackson & McKenzie 1984; Laana & Chen 1989; Byrne *et al.* 1992). Again, we re-examined earthquakes in the CMT and EHB catalogues to see whether the tectonic change associated with the Oman Line is revealed in an abrupt or gradual change in the earthquake depth distribution. In addition we wanted to see how depths obtained from body wave modelling compared with EHB depths in a region of known subcrustal seismicity.

We then re-examined published focal depths in the Tien Shan, another intracontinental collision belt, this time in central Asia (Fig. 12). This range has been influential in our views of continental tectonics because of the confirmed presence of earthquakes at depths of 40–50 km, near the probable depth of the Moho, in addition to the more common earthquakes at depths of 10–20 km (Chen & Molnar 1983; Nelson *et al.* 1987). The region has attracted considerable interest from seismologists, mainly because of international treaties related to nuclear testing, and we were anxious to see whether the additional data now available required any modification of these earlier views. We were conscious of the African experience, where seismicity occurs throughout the continental crust and is not restricted to the upper crust and the mantle.

Finally we looked at focal depths in north India and the Himalaya (Fig. 14). In the Shillong Plateau and southern Nepal, earthquakes at ~50 km depth have been interpreted to be in the mantle (Chen & Molnar 1990; Chen & Kao 1996), and others near the Himalayan front with depths of 50 km or more reported by the Harvard CMT or EHB catalogues apparently support this view. We re-examine the evidence for mantle focal depths in these and other earthquakes in the region, making use of the fact that we now have much better estimates of Moho depths, mostly from receiver function studies, than were available to Chen & Molnar (1983). The question of whether we can confirm that some earthquakes occur in the uppermost continental mantle is one of particular interest.

Table 1. The Zagros–Makran events analysed in this study. Published depths are listed from the EHB, Harvard CMT and USGS CMT catalogues, together with waveform-determined centroid depths. In the EHB column * indicates a depth which was fixed by the operator (flag FEQ), whereas all other EHB depths were freely determined in the EHB inversion (flag DEQ; see text). In the HRV column † indicates a depth that was fixed prior to the CMT inversion. Multiple events are indicated by an 'm' in the M_w column. In the method column, 'a' refers to full *P* and *SH* waveform inversion and 'b' to inversion for depth only. For class 'a' events, the strike, dip, rake and moment are from the minimum-misfit solution. For class 'b' events, the scalar moment is that published in the Harvard CMT catalogue. The events of 1985.02.02, 1985.03.27, 1992.03.29 and 1994.07.31 are discussed in the main text. Details of the other inversions are in the Appendix.

Date	Time	Lat. N	Lon. E	M_w	M_0	Depth (km)			*P*/*SH*	Fault Plane			Method	Region
						EHB	HRV	USGS		Strike	Dip	Rake		
1977 04 26	16:25	32.65	48.90	5.5	2.0e17	23	20		20				b	Zagros
1980 10 19	17:24	32.70	48.58	5.6	3.2e17	18	15		17	327	19	120	a	Zagros
1983 02 18	07:40	27.91	53.82	5.2	6.9e16	26	15†		6				b	Zagros
1985 02 02	20:52	28.36	52.97	5.6	2.8e17	16	22		11	128	37	91	a	Zagros
1985 03 27	02:06	31.59	49.92	5.1	7.3e16	53	84	150	15				b	Zagros
1988 08 30	17:30	29.96	51.72	5.1	3.0e16	24	15†		16				b	Zagros
1990 11 06	18:45	28.32	55.46	6.5	7.1e18	10	15	4	7	275	30	101	a	Zagros
1993 03 29	15:20	28.00	52.74	5.2	7.3e16	43	40		13				b	Zagros
1993 06 22	16:32	30.18	50.83	5.2	9.1e16	43	15		5	301	44	65	a	Zagros
1994 06 20	09:09	29.05	52.67	5.8	6.0e17	15	15	7	9	255	74	−3	a	Zagros
1994 07 31	05:15	32.69	48.42	5.5	2.0e17	41	18		14	288	17	90	a	Zagros
1998 08 21	05:13	34.30	48.20	4.9	3.3e16	22*	22		9				b	Zagros
1999 05 06	23:00	29.54	51.93	6.1	1.9e18		17	38	7	44	82	−6	a	Zagros
1977 03 22	11:57	27.60	56.42	6.0	1.5e18	15	10		12	77	34	112	a	Oman line
1977 12 10	05:46	27.68	56.60	5.6	2.9e17	13	15†		18	291	28	138	a	Oman line
1983 07 12	11:34	27.61	56.40	5.9	1.0e18	20	47	20	17	227	50	75	a	Oman line
1987 04 29	01:45	27.42	56.11	5.6	3.7e17	9	15		10	265	41	112	a	Oman line
1997 04 19	05:53	28.00	56.87	5.5	2.1e17	30	19	16	19	219	47	13	a	Oman line
1997 10 20	06:09	28.45	57.25	5.2	8.4e16	37	33†		28	244	19	47	a	Oman line
1980 04 28	07:04	27.55	64.48	5.5	2.1e17	50	43		54				b	Makran
1987 08 10	10:52	29.88	63.88	5.9	1.0e18	163	157		155	346	31	−50	a	Makran
1990 07 26	06:53	27.35	65.58	5.7	4.3e17	20	15†	11	8	216	76	44	a	Makran
1994 12 10	12:16	27.90	64.94	5.1	6.5e16	55	39	55	72				b	Makran
1998 06 10	08:30	28.22	58.49	5.3	9.5e16	89	105		85	117	7	−28	a	Makran

2 METHODS

Although the confinement of seismicity to the upper continental crust had been known in California for some time, it was not until the study by Chen & Molnar (1983) that its more general pattern was demonstrated. The reason for this was the difficulty in obtaining reliable focal depths outside dense local networks of seismic stations. Locations based on the arrival times of teleseismic *P* waves alone, the method routinely employed by the ISC, the USGS and its predecessors, suffer notoriously from a trade-off between origin time and depth, which can cause errors in focal depth of several tens of kilometres or even more. This effect arises because of the limited range of teleseismic ray parameters, with ray paths illuminating only a small part of the lower focal sphere (e.g. Jackson 1980). By the early 1980s the common use of teleseismic synthetic seismogram techniques, which can estimate centroid depths to typically ± 4 km, and the increasing number of temporary local seismic surveys allowed Chen & Molnar's (1983) compilation to be made. It is those synthetic seismogram techniques that we exploit here. Two types of analyses were performed, depending on the quality of the available waveform data.

2.1 Inversion for source parameters and depth

Where possible we used long-period *P* and *SH* waveforms to constrain the earthquake source parameters. We took digital broad-band records from stations of the Global Digital Seismographic Network (GDSN), deconvolved the station response from the records and then reconvolved them with the response of the old World Wide Standard Seismic Network (WWSSN) 15–100 long-period instruments, which have a bandwidth that is well suited for the resolution of shallow, moderate-sized events (e.g. McCaffrey & Nábělek 1987). Where broad-band data were not available, we used the original long-period digital data. Onset arrival times were measured either from the original broad-band data or from short-period records.

We then used the MT5 version of McCaffrey & Abers' (1988) algorithm, which inverts *P* and *SH* waveform data to obtain the strike, dip, rake, centroid depth, seismic moment and source time function. We always constrained the source to be a double couple. The procedure assumes that the source can be represented as a point (the centroid) in space, but not in time. The time history of displacement on the fault is represented by a source time function made up of a series of overlapping isosceles triangles. The seismograms are formed by the combination of direct *P* or *SH* waves with the surface reflections *pP*, *sP* and *sS* and near-source multiples. Amplitudes are corrected for geometrical spreading, and for anelastic attenuation using a Futterman *Q* operator with a value for t^* of 1.0 s for *P* and 4.0 s for *SH* waves. Uncertainties in t^* lead to uncertainties in source duration and seismic moment, but have only a small effect on centroid depth and source orientation. To avoid upper mantle triplications and interference from core phases, *P* waveforms are used in the distance range 30°–90° and *SH* waves in the range 30°–75°.

The inversion procedure adjusts the relative amplitudes of the source time function elements, the centroid depth, the seismic moment and the source orientation (strike, dip, rake) to minimize the misfit between observed and synthetic seismograms. We refer to this solution as the minimum-misfit solution. The covariance matrix associated with this solution usually underestimates the true uncertainties associated with the source parameters. A better estimate of the uncertainties is found by fixing some of the source parameters at values close to but different from those of the minimum-misfit solution, and seeing whether the match of observed to synthetic seismograms deteriorates (e.g. Molnar & Lyon-Caen 1989; Taymaz *et al.* 1991). We use this type of sensitivity analysis here. Changes in the depth and/or source time function will influence the width of the first pulse and the presence or absence of later pulses, while changes in the focal mechanism will influence the polarity and relative amplitudes of the pulses. The focal mechanism of an event is best constrained by stations that plot close to the nodal planes on the *P* or *SH* focal sphere.

Uncertainties in the seismic moment and centroid depth arise from errors in the source velocity model. Detailed velocity models are rarely known in the source regions of the earthquakes studied here. In general we used a velocity with an average *P* velocity of 6.0 km s^{-1} above the source and 6.8 km s^{-1} below the source, unless (in the case of a few earthquakes in the Makran, for example) the events were found to be genuinely subcrustal, in which case we used a 35 km crust of average *P* velocity 6.8 km s^{-1}, and a half-space mantle of *P* velocity 8 km s^{-1}.

2.2 Inversion for depth only

For some earthquakes there was insufficient good digital data for a full inversion for source orientation, depth, source time function and moment. In these cases we concentrated on constraining the depth by fixing the strike, dip and rake to suitable values (usually those given by the corresponding Harvard CMT solution) and allowing the depth, source time function and moment to vary.

In cases where only the depth was being investigated, we used the broad-band or short-period records when possible, as the depth phases are more easily distinguishable than in long-period records. In these cases we performed forward modelling of the vertical-component seismograms using the program WKBJ3 (Chapman *et al.* 1978). This program traces rays through a 1-D spherical earth using the WKBJ approximation for turning rays, allowing for the interference of rays and geometric spreading. We used the AK135 earth model (Kennett *et al.* 1995) for the generation of synthetics, and included only *P*, *pP* and *sP* waves. The synthetics were convolved with the responses of the individual broad-band or short-period stations, and corrected for attenuation using a Futterman operator with $t^* = 1$ before being compared with the data.

3 THE ZAGROS–MAKRAN REGION

We analysed a total of 24 events in the Zagros–Makran region (Table 1), 12 of them with $M_w > 5.5$. Of these, 16 had digital data of sufficient quality for a complete inversion of *P* and *SH* waveforms, and eight were analysed only to determine their depths. The EHB catalogue reported depths greater than 30 km for nine of the events we studied (of which four were in the Zagros with depths apparently greater than 40 km). The EHB catalogue contains a qualification of the earthquake depth determination. Locations in which the depth is free in the inversion are marked DEQ. Poorly determined depths are flagged XEQ, while other depths are fixed either by the inversion program (LEQ) or by the operator (FEQ). All nine of the

events reported deeper than 30 km were of type DEQ. The minimum-misfit fault plane solutions and depths for the events whose *P* and *SH* waveforms were inverted for source parameters, and our re-assessed depths for the others, are tabulated in Table 1. Details of the inversions and waveforms of events not discussed in the main text are contained in the Appendix.

Below we present a detailed description of four events in the Zagros region, partly to illustrate the data quality and techniques, and partly because these are particularly interesting earthquakes. The first and second examples (1994.07.31 and 1993.03.29) are of earthquakes that we re-determine as shallow (14 and 13 km) but which were reported to be much deeper (41 and 43 km) by the EHB catalogue. We analyse the first event using long-period *P* and *SH* waveform inversion, and the second using forward modelling of *P* waveforms. The third and fourth examples (1985.02.02 and 1985.03.27) were both reported by the Harvard CMT catalogue as normal faulting events, which are extremely unusual mechanisms to find in the Zagros fold-and-thrust belt. For the third event *pP* arrivals corresponding to a depth of 122 km were reported by the ISC, while the fourth event was reported at 53 km depth by the EHB catalogue and at 84 km by the Harvard CMT catalogue. We analyse the third event by long-period waveform inversion, and discover that it is a multiple event composed of two thrusting earthquakes. We use forward modelling of long-period *SH* waves to determine the depth of the fourth earthquake (15 km), and find some evidence for it possibly being a thrust faulting event.

3.1 1994 July 31, NW Zagros (M_w5.5)

All the observed *P* and *SH* waveforms used in the inversion for this event are shown in Fig. 2, along with the best-fit synthetic waveforms. Although available stations are restricted to the northern half of the focal sphere, they are well distributed within that, and the combination of *P* and *SH* waveforms constrains the inversion solution quite tightly, as we show

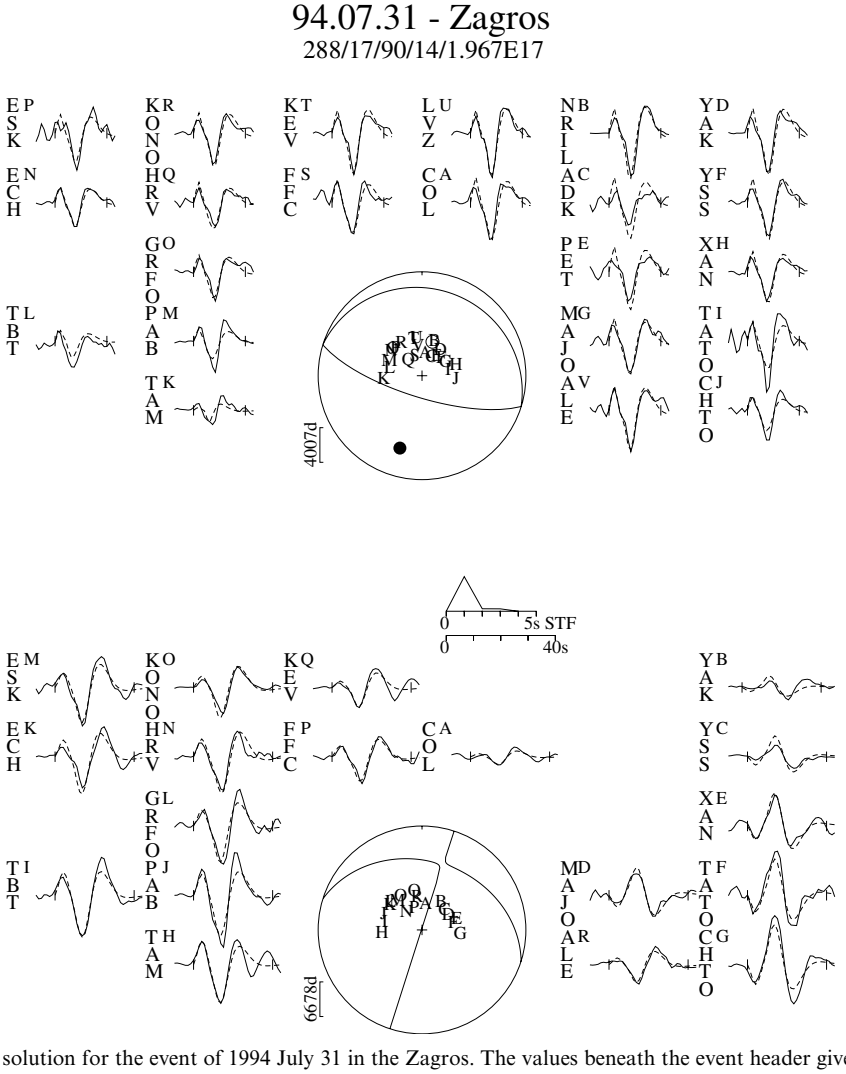

Figure 2. Minimum-misfit solution for the event of 1994 July 31 in the Zagros. The values beneath the event header give strike, dip, rake, depth in km and seismic moment in N m. This solution was calculated using a velocity model consisting of a 10 km thick layer with $V_P = 6.0$ km s^{-1}, $V_S = 3.45$ km s^{-1}, $\rho = 2.78$ g cc^{-1} over a half-space with $V_P = 6.8$ km s^{-1}, $V_S = 3.92$ km s^{-1} and $\rho = 2.91$ g cc^{-1}. The upper sphere shows the *P*-wave radiation pattern and the lower sphere that for *SH*. Both are lower-hemisphere projections. The station code by each waveform is accompanied by a letter corresponding to its position in the focal sphere. These are ordered clockwise by azimuth. The solid lines are the observed waveforms; the dashed lines are the synthetic waveforms. The inversion window is marked by solid bars at either end of the waveform. P and T axes within the sphere are represented by solid and open circles respectively. The source time function is shown below the *P* focal sphere, with the waveform timescale below it.

below. Synthetics were calculated for a 10 km thick layer with velocity $V_p = 6.0$ km s^{-1} over a half-space of $V_p = 6.8$ km s^{-1}, as described above. The minimum-misfit solution shows a thrust faulting mechanism with a simple time function of about 2 s duration and a depth of 14 km. The low dip (17°) of the shallow-dipping nodal plane is unusual in the Zagros, where high-angle (40–60°) reverse faults are common, but is similar to that of two other events nearby (1977.04.26 and 1980.10.19), also studied here (see Table 1).

The quality of the solution in Fig. 2 was assessed by tests, illustrated in Fig. 3, which shows the observed and synthetic *P* and *SH* seismograms at selected stations. The top line contains the minimum-misfit solution in Fig. 2. In line two the depth was held fixed at 41 km (as reported in the EHB catalogue) while all the other source parameters were allowed to be free to change in the inversion, which was started at the published CMT best-double-couple orientation (strike 309°, dip 41°, rake 114°). The result is a minimum in dip, depth, source time function and moment space, but is very much a worse fit than the minimum-misfit solution shown in the first line. In particular, there is no evidence in the *P* waveforms for the separation of the direct *P* and surface reflections, which would certainly be apparent if the depth were really 41 km (and which the inversion has attempted to minimize by rotating the nodal planes). The third and fourth lines show inversions in which the depth is held fixed at 18 and 10 km, while all other source parameters are free. At 18 km (line 3) the fits at LVZ (*P*), TATO (*SH*) and PAB (*SH*) in the third line are significantly worse than in line 1. The fits in line 4 (depth 10 km) are not significantly worse than in line 1, but the inversion has compensated for the shallow depth by requiring a double pulse to the source time function, which is possible but not very likely for an event of this size (M_w5.5). If the time function is required to be short as well as the depth fixed at 10 km (line 5), the fit at all stations deteriorates. We conclude that the uncertainty in our estimate of the centroid depth for this earthquake (14 km) is unlikely to be greater than ± 4 km.

This earthquake, therefore, is significantly shallower than reported by the EHB catalogue (14 ± 4 versus 41 km). Note that for an earthquake of this size ($M_0 = 2 \times 10^{17}$ N m) the source dimension is unlikely to exceed ~ 5 km, which would be the maximum allowable difference between the position of rupture nucleation detected at short periods and the centroid position estimated at long periods. The difference between the EHB depth and our re-determined centroid far exceeds that.

3.2 1993 March 29, S Zagros (M_w5.2)

The teleseismic waveform data available for this relatively small (M_w5.2) event were insufficient for complete body waveform inversion, so we performed forward modelling of the broad-band records directly using WKBJ3. We assumed a source orientation given by the Harvard CMT mechanism, which was a thrust with strike 104°, dip 28°, rake 72° , similar in orientation to many other known earthquakes nearby (e.g. Baker *et al.* 1993). As the earthquake was relatively small we expect a time function of only 1–2 s duration. To generate synthetic seismograms we used an impulse time function, but

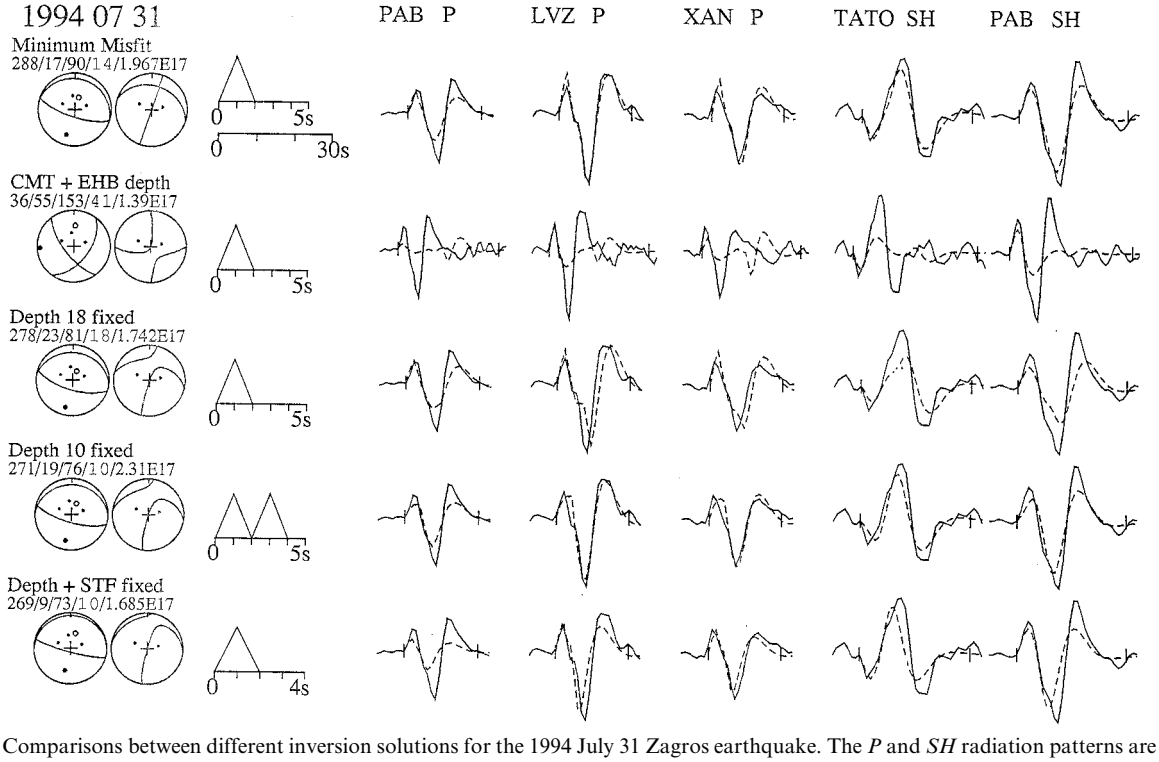

Figure 3. Comparisons between different inversion solutions for the 1994 July 31 Zagros earthquake. The *P* and *SH* radiation patterns are shown in the first column, with the strike, dip, rake, depth in km and scalar moment in N m above the two focal spheres. The source time function for each solution is in the second column, followed by the observed and synthetic waveforms. Line 1: the minimum-misfit solution; line 2: the result of an inversion started from the published Harvard CMT solution with the fixed EHB depth of 41 km; lines 3–5: tests for the uncertainty in the depth; in all these inversions the depth was held fixed and all other parameters were free to change. In line 5 the duration of the source time function was also held fixed.

with the addition of attenuation (a Futterman operator with $t^{\star}=1$ s for P waves) the effect on the synthetic seismograms is equivalent to a time function of ~ 1 s.

Fig. 4 shows the comparison between data and synthetics for two stations, XAN (Δ 48°, Az 068°) and YSS (Δ 70°, Az 047°). In order to use records as similar as possible to those on which the station operators had identified their reported phases, we transformed the original broad-band records into records with the WWSSN short-period response. The seismograms are aligned on the first prominent trough in the waveforms after the P arrival time published by the ISC. The synthetics calculated for a depth of 13 km (our preferred depth, see Table 1) mirror the essential features of the short-period seismograms above them. One early peak that is present at both stations (~ 2 s after the P arrival at XAN and ~ 4 s after the P arrival at YSS) is not fitted by the synthetic seismograms. We cannot fit both this early peak and the group we are currently fitting by using only P, pP and sP rays. Also shown in Fig. 4 are synthetics calculated for the EHB reported depth of 43 km. The position of the pP peak in the synthetic corresponds to a pP arrival time identified by the ISC at XAN. A depth of 43 km for this event would, however, ignore the more prominent arrivals at ~ 15–18 s at both stations, arrivals that had been reported to the ISC, but not identified as depth phases.

Despite the poor quality of the data available, we conclude that this earthquake was shallow ($\sim 13 \pm 3$ km) rather than at ~ 40 km depth as reported by both the EHB and HRV catalogues.

3.3 1985 February 2, S Zagros (M_w5.6)

This earthquake has a wide range of depths reported for it: 16 km by the EHB catalogue, 22 km by the Harvard CMT catalogue and 44 km by the ISC, who also report a depth of 122 km based on pP–P arrival times. In addition, Harvard give a CMT solution that is nearly a pure double-couple source (eigenvalues of 1.81, 0.03 and -1.85, all $\times 10^{17}$ N m) indicating normal faulting in the crust (22 km depth) with a strike parallel to the fold-and-thrust belt, which would be extremely interesting if it were confirmed. Finally, several stations in the ISC bulletin quote S-wave arrivals with unusually large traveltime residuals of between $+20$ and $+30$ s.

In our analysis below we show that this earthquake was probably a double event, consisting of a small foreshock followed around 25 s later by a larger, thrust-faulting earthquake in roughly the same place. Both subevents are at shallow depths. We suspect that the S phase reported with a $+20$ to $+30$ s residual is actually from the second subevent, and that it is the P arrival from the second subevent that was mistaken for the pP arrival for the first subevent, explaining the apparent depth of 122 km from pP–P times.

Observed P and SH seismograms and synthetics from our preferred inversion solution are shown in Fig. 5. The amplitudes of the observed P onsets are comparable with the noise level in the long-period waveforms, so the arrival times indicated by the arrows were taken from short-period records, which were clear. Baker (1993) showed that on the stacked short-period array data at Eskdalemuir (EKA), Yellowknife (YKA) and Warramunga (WRA), the P onsets are impulsive and unambiguously compressional. These polarities conflict with the expected dilatational first motions at these stations if the focal mechanism was indeed normal faulting, but are compatible with a thrust parallel to the regional strike of the Zagros folds nearby. At all stations there is a large pulse about 25 s after the initial P onset time, and this pulse has the characteristic inverted W shape of a shallow (~ 10 km depth) reverse faulting earthquake of magnitude ~ 6 (e.g. Jackson & Fitch 1981).

In our waveform modelling the mechanism of the first subevent was fixed with the nodal planes in the same orientation as the Harvard CMT solution, but with the rake changed so that the mechanism is now a thrust (compatible with the compressional onsets at ESK, YKS and WRA). The first event is very small, with a moment less than a tenth of that of the second subevent, so it makes only a very small contribution to the form of the synthetic seismograms. The second subevent

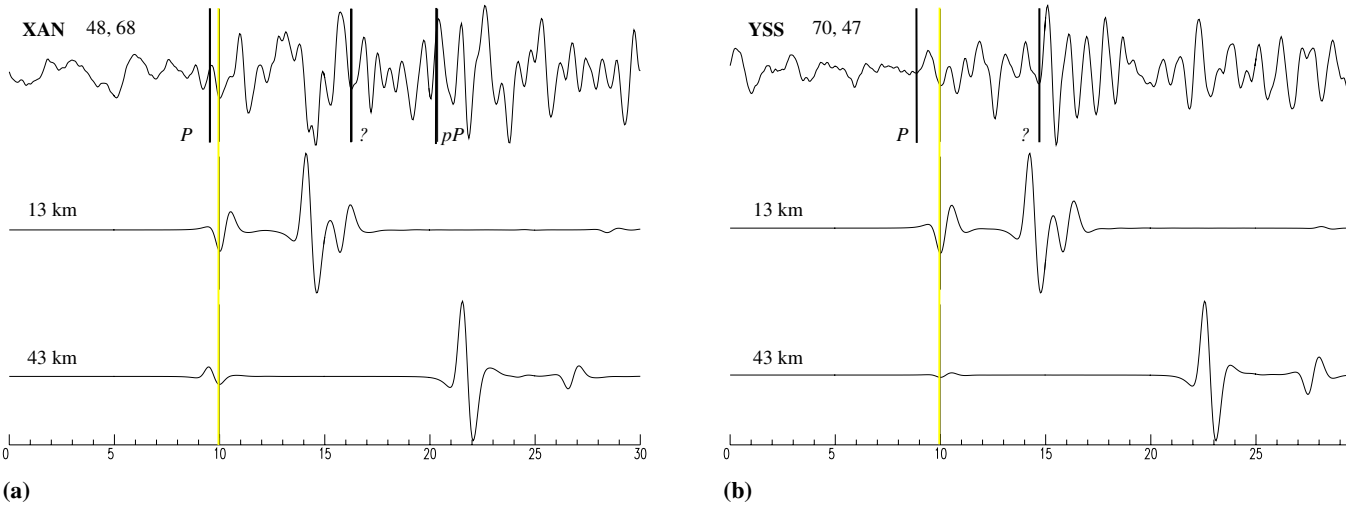

Figure 4. Forward modelling of the focal depth for the 1993 March 29 Zagros earthquake using WKBJ3 for (a) station XAN (Δ 48° and Az 068°) and (b) station YSS (Δ 70° and Az 047°). For both stations the first trace is the broad-band vertical record, which has been transformed to one with the WWSSN short-period response, with the ISC time picks shown as thick black lines. The ISC phase identifications for the picks are also shown, with unidentified phases shown by question marks. The second trace is a synthetic computed for a depth of 13 km, and the third trace is a synthetic computed for the EHB reported depth (43 km).

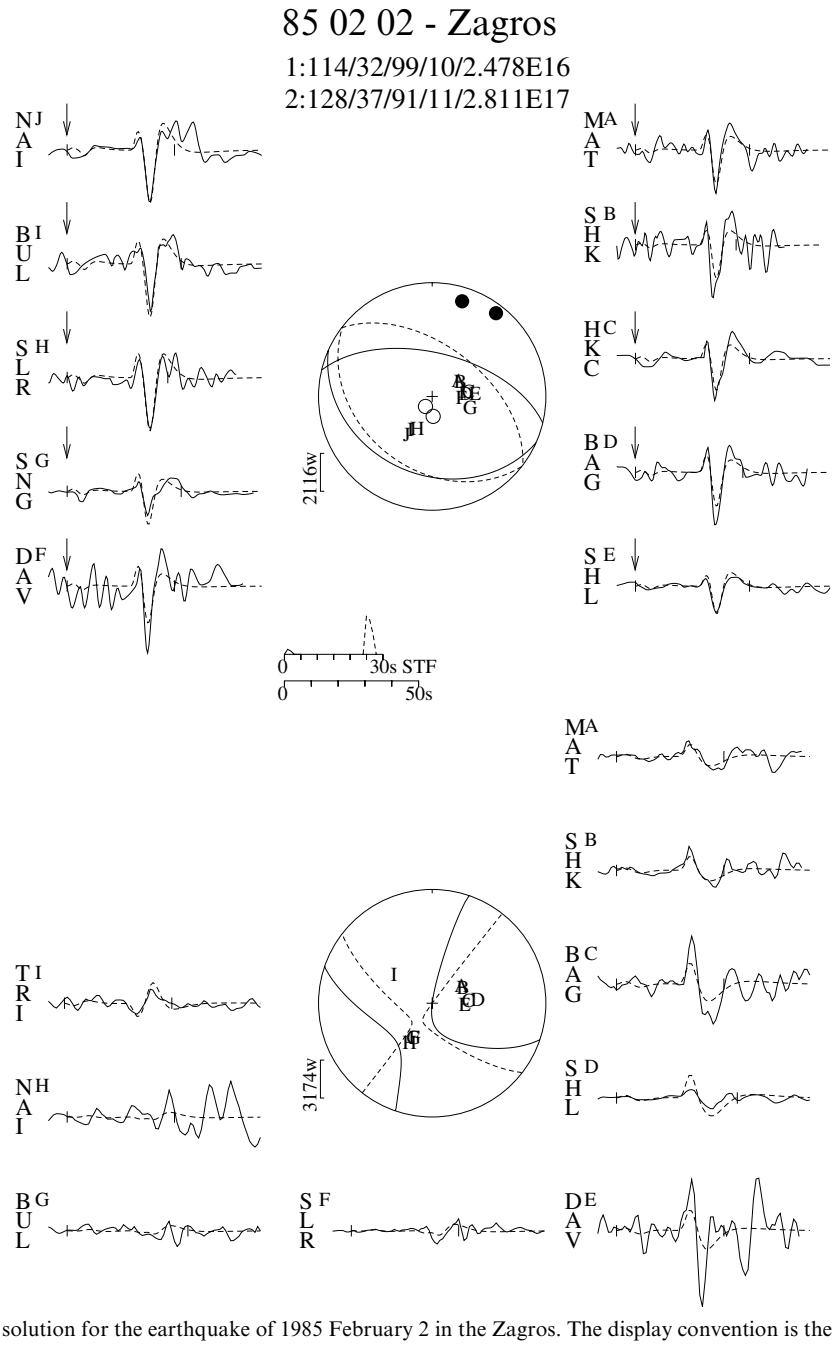

Figure 5. Minimum-misfit solution for the earthquake of 1985 February 2 in the Zagros. The display convention is the same as in Fig. 2. There are two subevents in this case. The two mechanisms are printed under the header and the second source is represented as a dashed line within the focal sphere. The source time function indicates two distinct ruptures, the second occurring ~22 s after the onset of the first. Arrows mark the *P* arrival time determined from short-period records.

was modelled from the data, inverting for source orientation, moment, depth and origin-time offset from the first subevent. This gives a thrust mechanism for the second event with planes that dip at similar angles to the CMT solution, but with the slip vector rotated clockwise by about 15°. We obtained this solution using a velocity model consisting of a 7 km layer (V_p 6.0 km s^{-1}) over a half-space (V_p 6.8 km s^{-1}).

Fig. 6 shows tests to illustrate the robustness of our modelling. The top line shows the fit of *P* and *SH* waveforms at selected stations obtained for our preferred solution in Fig. 5. The second line shows the fit obtained for the Harvard CMT solution. The first-motion amplitudes are much larger than those actually observed and this mechanism fails to account for the second pulse seen at all stations on the *P* waveforms. The solution in the third line fixes the fault orientation at that of the Harvard CMT solution and investigates the possibility that the second pulse is the result of the surface-reflected phases *pP*, *sP* and *sS*. We have allowed the depth and moment to vary in this inversion. The plots show that, for a depth of about 85 km, it is possible to obtain a second pulse with the correct polarity and onset time for the *P* waveforms. However, the amplitudes of the first motions are larger than observed, and the fit is

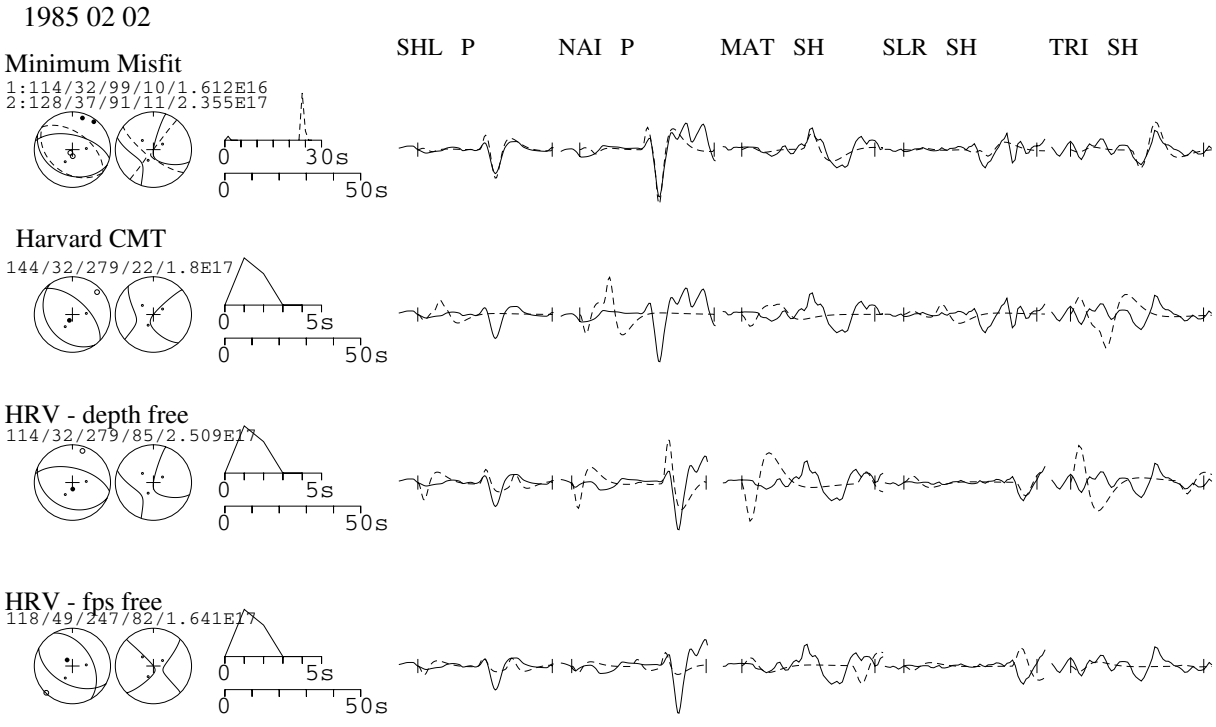

Figure 6. Comparison of possible solutions for the 1985 February 2 Zagros earthquake. The display convention is the same as in Fig. 3. Line 1 shows the minimum-misfit solution in Fig. 5. Line 2 shows a solution in which the source orientation and depth were fixed to the Harvard CMT solution. In line 3 the source orientation was held fixed at the Harvard CMT solution, but the depth was free to change. In line 4 both the source orientation and depth were allowed to vary from the Harvard starting model.

also noticeably less good for the *SH* waveforms (the onsets at MAT and TRI are much larger than are observed and the *sS* phases are smaller than those required to match the observed waveforms). The fourth line shows the results of a similar test where the fault orientation is also allowed to vary. This results in a better fit to the amplitudes of the first motions but fails to provide an adequate fit to the second pulse.

Therefore, we believe that this earthquake consists of two subevents with shallow depths. The mechanism of the first is too small to be modelled using body waves, but compressional arrivals on stacked array data suggest thrusting, not normal faulting. The second subevent occurred 25 s after the first. Its mechanism can be constrained by the modelling of body waves, which confirms a thrust mechanism and a depth of $\sim$11 km, comparable with the EHB depth of 16 km. The first event was too small to determine formal errors; for the second event, the uncertainty in depth is about $\pm$4 km. In our interpretation neither the fault type or depth(s) of this earthquake are unusual in the Zagros.

3.4 1985 March 27, NW Zagros (M_w5.1)

The Harvard CMT catalogue reports a reasonably good double-couple solution for this event (eigenvalues of 5.50, 0.81 and -6.35, all $\times 10^{16}$ N m), indicating normal faulting and a centroid depth of 84 km, both of which would be extremely surprising in the Zagros if they were to be confirmed. The EHB catalogue reports a depth of 53 km.

The long-period *P* waveforms for this event were barely detectable above the noise, but the long-period *SH* waveforms had roughly double the amplitude of *P*, and could be used for forward modelling and testing of various source geometries. Fig. 7 shows synthetic and observed *SH* waveforms in order to compare three different source models for this earthquake. The first model (a) is that reported in the Harvard CMT catalogue. The synthetics fit the amplitude and width of the first peak at four out of the six stations, and also try to fit a smaller, second peak, most visible at RSON, as an *sS* arrival. It is this second peak at RSON that lends support to the Harvard CMT depth of 84 km. However, the second peak is not matched at eastern stations (SHIO, CHTO, NWAO), nor are the amplitudes and widths of the first pulses matched at CHTO and NWAO. The second model (b) in Fig. 7 retains the Harvard CMT normal faulting mechanism but at a shallower depth of 15 km. In this model the amplitude and width of the first peak are fitted well at all stations, and any later arrivals are ignored. The third model (c) is a thrusting mechanism (strike 115°, dip 65°, rake 65°, similar to other focal mechanisms nearby) at a depth of 15 km. Once again the first pulse is well fitted both in amplitude and width at all stations, and the second pulse is ignored.

Given the level of noise in these records (approximately half the *SH*-wave amplitude), it is quite possible that the second pulses at RSNO, RSNY and GRFO are due either to noise or to some phase other than *sS*. To investigate this further, we show in Fig. 8 three vertical-component array stacks for this earthquake, taken from Baker (1993). The noise level in these stacks is significantly lower than that for the single seismograms, which means that the *P*-wave onsets are visible. The expected *pP* and *sP* arrival times for a depth of 84 km are shown on the traces and do not correspond to significant features in the seismograms. Therefore, we conclude that this event is more likely to have had a shallow depth, occurring at $\sim$15 km.

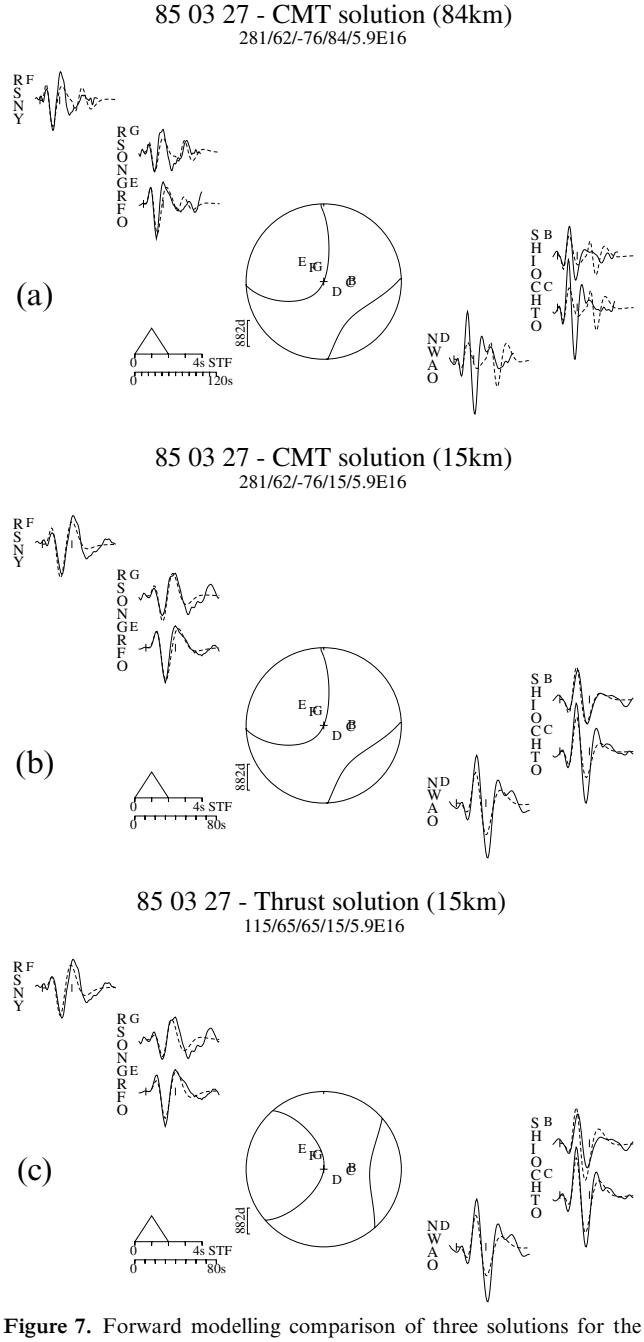

Figure 7. Forward modelling comparison of three solutions for the 1985 March 27 earthquake in the Zagros. Only the *SH* focal spheres are shown. The display convention is the same as in Fig. 2. (a) The CMT focal mechanism (a normal faulting earthquake) at the CMT-determined depth of 84 km. (b) The same normal faulting mechanism at 15 km depth. (c) A thrusting mechanism also at 15 km depth. Note that the timescales in (b) and (c) are different from (a).

As Fig. 7(c) shows, the long-period *SH* data can be fitted just as well by a thrust as by a normal faulting mechanism. The first arrivals on the stacked array data are all compressional (Fig. 8), which is consistent with a thrust but not with a normal fault. The available data do not allow us to constrain the source parameters tightly, but seem to us to favour a thrust faulting mechanism with a shallow (10–15 km) depth, which would not be at all unusual, rather than a deep normal faulting event, which would be unique in the NW Zagros.

3.5 The Zagros–Makran region: summary

The results of our investigations in this region are summarized in Table 1 and Figs 9 and 10, and when combined with other studies of additional earthquakes using the same techniques (Table 2) can be used to form a clearer picture of the focal depth distribution. Of the five Zagros earthquakes in Tables 1 and 2 reported with depths of greater than 40 km by the EHB catalogue, all are shown to have shallow depths of approximately 15, 13, 5, 14 and 7 km. Two of these earthquakes were also given depths of 40 and 84 km by the Harvard CMT catalogue. The two apparently normal faulting events reported by the Harvard CMT catalogue (1985.02.02 and 1985.03.27, discussed above) are more likely to have had thrust faulting mechanisms. There is no evidence in the events studied here or by others using the same methods (Table 2) for earthquakes significantly deeper than 20 km in the Zagros, in agreement with local microearthquake surveys. It is clear that significant mislocations in depth can occur in the EHB catalogue, even amongst good-quality hypocentres. We discuss possible reasons for these discrepancies later (Section 6.1). Although the EHB catalogue reports other small Zagros earthquakes with depths greater than 50 km (Fig. 1), we view these depth determinations with scepticism. Our image of the depth distribution in the Zagros is thus unchanged from the days of Chen & Molnar (1983), with earthquakes largely confined to the upper crust (Fig. 10a) and no evidence in the form of mantle earthquakes for active subduction.

Near the Oman line there is some indication that the seismicity extends to greater depths in the crust, but the sample is quite small (Fig. 10b). More significant is one earthquake whose depth of 28 km, deeper than any in the Zagros, was confirmed by long-period *P* and *SH* waveforms. We show a selection of those waveforms in Fig. 11 to emphasize how different they are from the more common earthquakes at 10–15 km (compare with Fig. 2). One genuine shallow normal faulting event (1987.12.18 at 10 km depth) near the Oman Line has also been confirmed by *P* and *SH* waveforms (Fig. 9c; Baker 1993). The earthquake of 1970.11.09 at 100 km depth (Fig. 9c) probably occurred in the subducting slab beneath the Makran, and is discussed below.

It has been known for some time that the Makran region experiences earthquakes with depths genuinely deeper than 50 km. Of interest here is how the EHB and CMT depths compare with those confirmed by waveform modelling. Tables 1 and 2 list nine earthquakes whose depths are estimated to be in the range 50–170 km by the EHB catalogue. For eight of these events, waveform analysis, either by *P* and *SH* modelling or by the identification of *pP* and *sP* on short-period records (relatively easy at these depths), confirms the depths to be within ± 10 km of the EHB estimates. Only in one case (1994.12.10) is the discrepancy greater (17 km). The Harvard CMT catalogue estimates two depths to be greater than 100 km, both of which are similarly confirmed to within ± 15 km (Table 1). The tectonic view of the Makran expounded by Jackson & McKenzie (1984), Laana & Chen (1989) and Byrne *et al.* (1992) is thus unmodified by these results, with earthquakes in the upper crust and also within a subducting slab dipping north at $\sim 26^\circ$ (Figs 9b and 10c and d). The deep earthquake of 1970 November 9 (100 km) appears to lie on the down-dip projection of this slab, at its western edge (Fig. 10d).

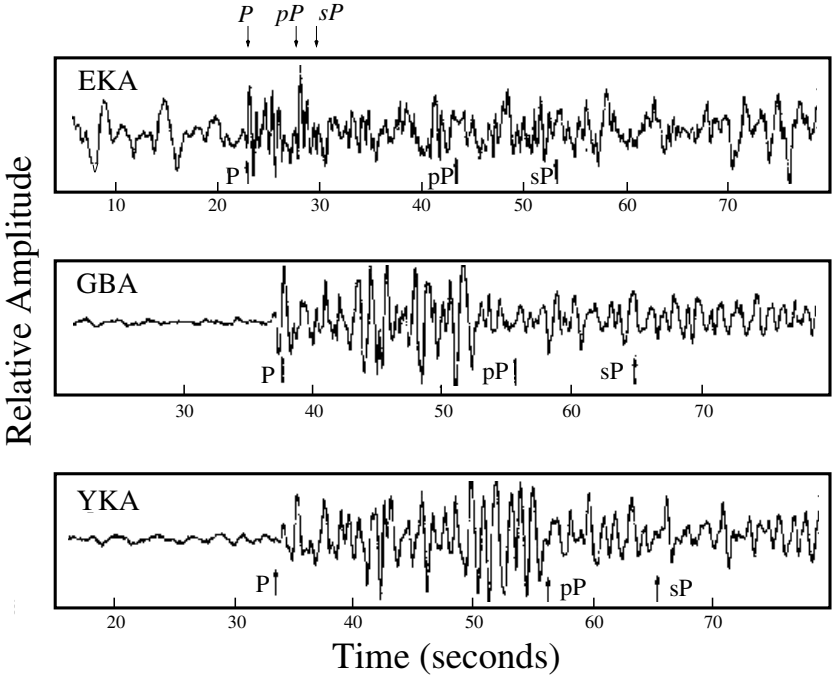

Figure 8. Stacked array seismograms for the 1985 March 27 Zagros event. The arrows show the expected *P*, *pP* and *sP* arrival times for an event depth of 84 km (in bold, below each trace) and 15 km (in italics, above the top trace). This figure was modified from Baker (1993).

4 THE TIEN SHAN REGION

The Tien Shan form an active intracontinental mountain belt within central Asia. In this study we concentrate on the region north of 40°N, away from the deep mantle seismic zones of the Pamir and Karakoram that represent subducted slabs penetrating to ~300 km (e.g. Fan *et al.* 1994; Pegler & Das 1998). The EHB catalogue shows few earthquakes with good-quality hypocentres deeper than 50 km in this region (Fig. 12), in contrast to the Zagros (Fig. 1). Nevertheless, the Tien Shan has been influential in our views of focal depth distribution on the continents because of confirmed depths that are certainly greater than 20 km, again in contrast to the Zagros. Chen & Molnar (1977) found two earthquakes (1965.11.13 and 1973.06.02) at ~50 and ~30 km by identifying *pP* reflections on long-period WWSSN records. These were later confirmed at

Table 2. Zagros–Makran events whose source parameters have been determined by *P* and *SH* waveform inversion in other studies. In the HRV column † indicates a depth that was fixed prior to the CMT inversion. Multiple events are indicated by an 'm' in the M_w column. The references are to: JQ79, Jacob & Quittmeyer (1979); JM84, Jackson & McKenzie (1984); BJP93, Baker *et al.* (1993); B93, Baker (1993); LC89, Laana & Chen (1989).

Date	Lat. N	Lon. E	M_w	Depth (km)			Region	Ref.
				P/*SH*	EHB	HRV		
1968 06 23	29.75	51.26	5.5	9	32		Zagros	BJP93
1971 04 06	29.78	51.88	5.2	6	5		Zagros	BJP93
1972 04 10	28.39	53.74	6.7 m	9	6		Zagros	BJP93
1974 12 02	28.09	55.86	5.2	7	49		Zagros	B93
1976 04 22	28.69	52.12	5.6	7	23	15†	Zagros	BJP93
1977 04 06	31.96	50.67	5.9	6	11	10	Zagros	B93
1985 08 07	27.86	53.04	5.4	17	11	15†	Zagros	B93
1986 07 12	29.91	51.56	5.5	4	7	33†	Zagros	BJP93
1986 12 10	29.88	51.56	5.3	8			Zagros	BJP93
1988 08 11	29.95	51.57	5.5	7	15	15	Zagros	BJP93
1988 08 11	29.89	51.66	5.8	9	15	15†	Zagros	BJP93
1988 12 06	29.89	51.63	5.6	10	12	37	Zagros	BJP93
1987 12 18	28.15	56.66	5.8	10	21	15	Oman line	B93
1968 08 02	27.55	60.90	5.7 m	74	67		Makran	JQ79
1969 11 07	27.81	59.98	6.1 m	62	75		Makran	JQ79
1970 11 09	29.50	56.79	5.5	100	98		(Makran)	B93
1972 11 17	27.37	59.11	5.4 m	65	64		Makran	JM84
1983 04 18	27.77	62.06	6.6	65	63	51	Makran	LC89
1990 09 26	29.07	60.89	5.5	8	5	15†	Makran	B93

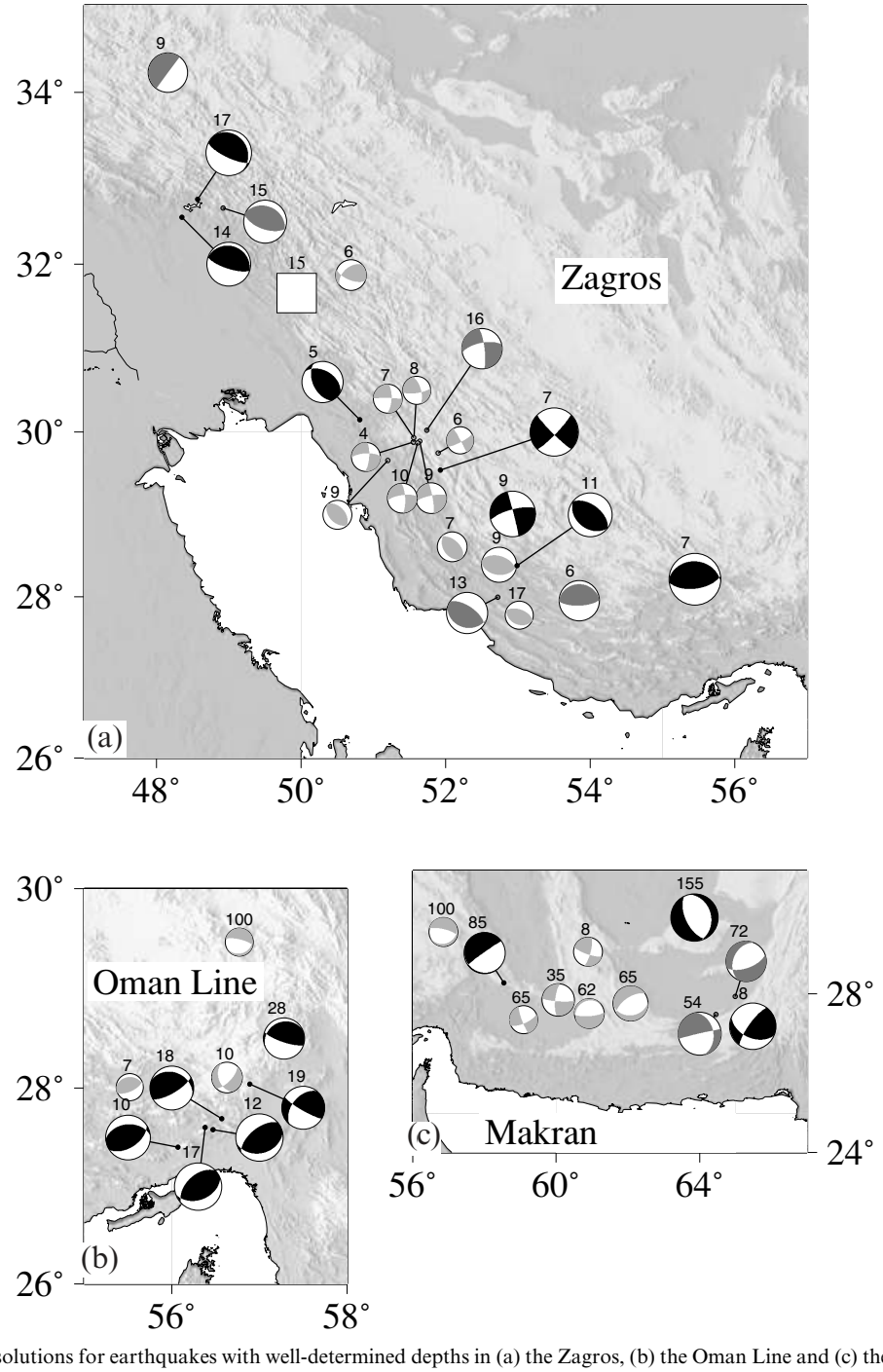

Figure 9. Fault plane solutions for earthquakes with well-determined depths in (a) the Zagros, (b) the Oman Line and (c) the Makran regions. Black symbols correspond to events for which *P* and *SH* waveform inversion was performed in this study. Dark grey symbols refer to events for which only the depth was determined in this study; the mechanisms shown for these events are those published in the Harvard CMT catalogue. Light grey symbols refer to events whose mechanism and depth were determined by *P* and *SH* waveform inversion in other studies (see Table 2). The white square represents the 1985 March 27 earthquake (see text for details). The depth in km of each event is shown above the corresponding symbol. The 100 km deep 1970.11.09 event is shown in both (b) and (c).

44 and 26 km using long-period *P* and *SH* body wave analysis by Nelson *et al.* (1987), who found another (1979.9.25) at 40 km. At the time of Chen & Molnar's (1983) review, it was unclear whether earthquakes occurred in the mantle lithosphere beneath the Tien Shan. Now, with many more accurately determined focal depths and with better estimates of crustal thickness, we re-examine that question.

More than 60 earthquake centroid depths in this region have been constrained by teleseismic and regional *P* and *SH* body wave modelling. Most are shallower than 20 km, but 10 have depths of 20–44 km (Fig. 13a and Table 3), in contrast to the Zagros (Fig. 10a). Broad-band receiver functions have been used to estimate Moho depths of 45 km beneath Urumqi (WMQ) and 42–60 km beneath the KNET network in Kyrgyzstan

Table 3. Tien Shan events with waveform-determined depths of 20 km or more in the Tien Shan. In the EHB column * indicates a depth that was fixed by the operator (flag FEQ), whereas all other EHB depths were freely determined in the EHB inversion (flag DEQ; see text). In the method column 't' refers to teleseismic waveform inversion and 'r' refers to regional waveform inversion. References are to: FNW94, Fan *et al.* (1994); GHA98, Ghose *et al.* (1998); NMM87, Nelson *et al.* (1987).

Date	Lat. N	Lon. E	M_w	Depth (km) *P*/*SH*	Depth (km) EHB	Ref.	Method
1965 11 13	43.84	87.76	6.3	44	51	NMM87	t
1973 06 02	44.14	83.59	5.5	26	22	NMM87	t
1979 09 25	45.09	76.98	5.4	40	41	NMM87	t
1982 05 06	40.14	71.53	5.5	20	30	NMM87	t
1988 01 06	39.68	75.50	5.3	37	26	FNW94	r
1991 10 31	40.14	72.82	5.1	31	19	GHA98	r
1993 09 20	42.57	76.05	3.8	21		GHA98	r
1995 02 20	41.18	72.40	4.9	22	40	GHA98	r
1995 11 03	40.17	73.77	4.4	20	48	GHA98	r
1996 06 01	41.35	76.97	4.2	22	26*	GHA98	r

(Mangino *et al.* 1999; Kosarev *et al.* 1993; Bump & Sheehan 1998). Thus, at least in some parts of the Tien Shan, there is no doubt that the lower continental crust is seismically active, although with relatively few earthquakes. However, there is no clear evidence of earthquakes in the continental mantle lithosphere north of 40°N. The two deepest known earthquakes remain those of 1965.11.13 (44 km, close to station WMQ) and 1979.09.25 (40 km) confirmed by Nelson *et al.* (1987), and we were unable to find any more recent examples with comparable depth. The focal depth distribution in the Tien Shan is clearly different from that in the Zagros.

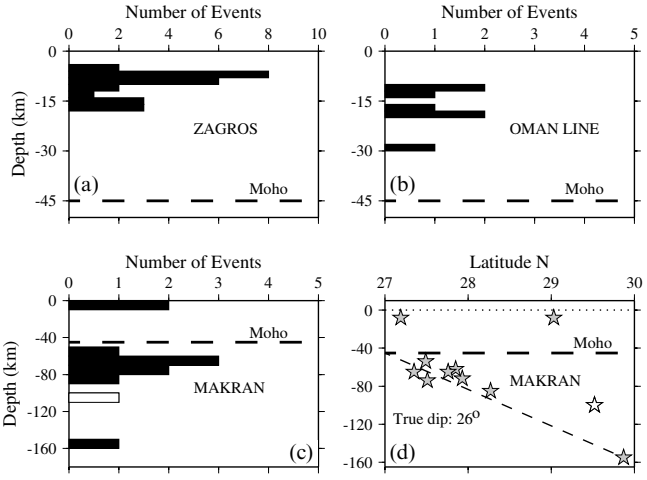

Figure 10. Histograms showing the focal depth distributions of earthquakes in Tables 1 and 2 in (a) the Zagros, (b) the Oman Line and (c) the Makran regions. (d) A N–S cross-section of the Makran showing the extrapolated position of the slab. The approximate Moho depths are shown in all figures, based on receiver function studies in the southern Zagros (K. Priestley, personal communication, 1999). The white symbols in (c) and (d) refer to the 1970.11.09 event, which we interpret as lying on the western edge of the subducting slab.

5 NORTHERN INDIA

Our main interest in this region is in whether there is unequivocal evidence for earthquakes within the mantle lithosphere of the Indian shield. There is certainly evidence for seismicity in the lower crust. The 1997.05.21 earthquake at Jabalpur, on the Indian shield south of the Ganges basin (Figs 14 and 15c and Table 4), had a well-determined centroid depth of 35 km, with many aftershocks also at depths of

Table 4. Earthquakes with waveform-determined depths of 20 km or more in peninsular India, the central Himalayas and southern Tibet. In the method column 'd' refers to depths determined from short-period depth phases, while 't' and 'r' are depths determined from teleseismic or regional waveforms. References are to: C81, Chen *et al.* (1981); MC83, Molnar & Chen (1983); E87, Ekström (1987); CM90, Chen & Molnar (1990); CK96, Chen & Kao (1996); ZH96, Zhu & Helmberger (1996).

Date	Lat. N	Lon. E	M_w	Depth (km) *P*/*SH*	Depth (km) EHB	Ref.	Region	Method
1973 08 01	29.60	89.13	4.9	85	93	MC83	Tibet	t
1976 09 14	29.78	89.53	5.9	90	103	C81	Tibet	t
1991 12 21	27.89	87.96	4.7	70	45	ZH96	Tibet	r
1992 03 07	29.62	89.19	4.2	80	79	ZH96	Tibet	r
1992 04 04	28.14	87.96	4.8	80	49	ZH96	Tibet	r
1968 08 18	26.41	90.60	5.1	29	28	CM90	Himalaya	d
1971 07 17	26.39	93.16	5.5	36	43	CM90	Himalaya	t
1980 11 19	27.39	88.79	6.0	44	44	E87	Himalaya	t
1963 06 19	24.97	92.06	6.0	52		CM90	Shillong	d
1963 06 21	25.13	92.09	6.0	38		CM90	Shillong	d
1968 06 12	24.83	91.89	5.3	41	44	CM90	Shillong	d
1988 02 06	24.68	91.51	5.9	31	30	CM90	Shillong	t
1988 08 20	26.73	86.59	6.7	51	61	CK96	Nepal	t
1996 04 01	31.50	73.44	5.5	38	92	Here	Nilore	t
1997 05 21	23.10	80.12	6.0	35	39	B97	Jabalpur	t

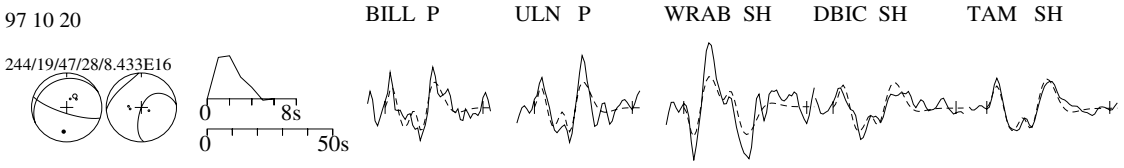

Figure 11. Selected waveforms from the minimum-misfit solution for the earthquake of 1997 October 20 at a depth of 28 km near the Oman Line (Fig. 9b). The full solution is given in the Appendix.

35–40 km (Battacharya *et al.* 1997; Acharyya *et al.* 1998). The Moho in the Jabalpur region is known to be at 40–44 km from wide-angle reflection and refraction studies (Murty *et al.* 1998). An earthquake on 1996.04.01 in the Punjabi foreland of the NW Himalaya had a centroid depth determined at 38 km (Fig. 15a) and occurred less than 200 km south of the GDSN station at Nilore (NIL), where receiver functions indicate a Moho depth of 50–54 km (Fig 15b).

Chen & Kao (1996) reported an earthquake at 51 km near Udaypur in Nepal on 1988.08.20 (Fig. 14), suggesting that it occurred in the uppermost mantle of the Indian shield. With the better information on crustal thickness now available at Jabalpur and Nilore we suspect that this may in fact have occurred in the lower crust. If the relatively undeformed Indian shield near Jabalpur has a Moho depth of 40–44 km, then 500 km further north, beneath the frontal thrusts of the Himalaya where the shield has certainly been bent down to form the Ganges basin (e.g. Lyon-Caen & Molnar 1983; McKenzie & Fairhead 1997), it seems probable to us that the Moho could quite easily be at 50–55 km, especially since that is the Moho depth determined at Nilore.

A similar argument applies to the earthquakes reported by Chen & Molnar (1990) beneath the Shillong Plateau (Fig. 14), where the Precambrian basement of the Indian shield is uplifted 1000 m above the foreland of the eastern Himalayas. Several focal depths in the range 30–40 km are constrained by teleseismic waveforms (Chen & Molnar 1990) and microearthquakes are largely confined to the range 15–35 km (Kayal & Zhao

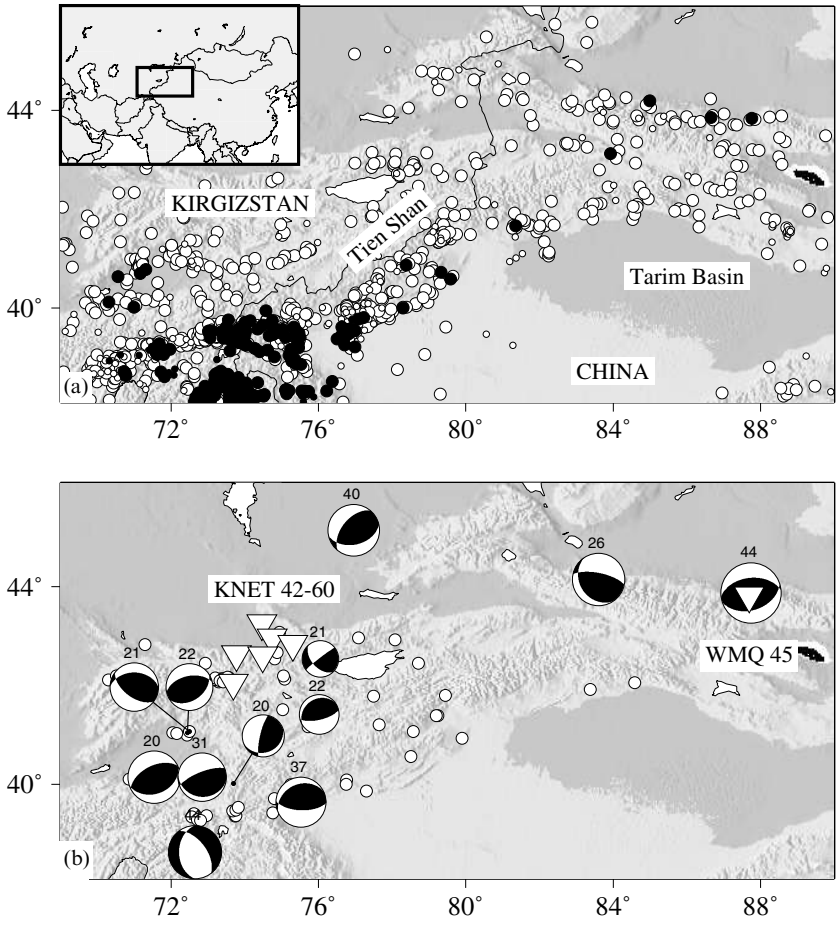

Figure 12. The Tien Shan region. (a) Seismicity taken from the EHB catalogue, with events reported to be at 50 km depth or deeper shown in black. Large circles are those events whose depths were freely determined (flag DEQ), while small circles are events whose depth was fixed by the operator (flag FEQ; see text). The geographical location of the region is shown in the inset map. (b) Fault plane solutions of earthquakes with depths greater than 20 km analysed by waveform inversion methods in other studies (Table 3). The depths in km are shown above the focal mechanisms. Events from the same studies with depths less than 20 km are shown as white circles. White triangles show the position of broad-band seismometers in the KNET array and at Urumqi (WMQ), under which Moho depths of 42–60 km and 45 km have been determined from receiver functions (Bump & Sheehan 1998; Kosarev *et al.* 1993; Mangino *et al.* 1999).

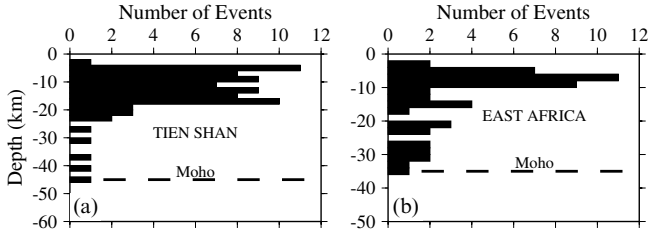

Figure 13. Histograms showing the distributions of well-determined focal depths in (a) the Tien Shan and (b) East Africa. The Tien Shan histogram contains all the events plotted in Fig. 12, while the East Africa histogram contains all the continental events discussed by Foster & Jackson (1998). The Moho is shown at 45 km (Mangino *et al.* 1999) in (a) and at 35 km (Zhao *et al.* 1997; Foster & Jackson 1998) in (b).

1998). Chen & Molnar (1990) reported one focal depth at ~52 km, based on the identification of *pP* and *sP* on short-period records. The Moho depth beneath the Shillong Plateau is not well known. The EGM96 gravity field (Lemoine *et al.* 1996) shows that the plateau is mostly compensated, with a flexural gravity low in front of it indicating a relatively small elastic thickness in this part of the foreland (see Plate 5 of McKenzie & Fairhead 1997). If the undeformed crustal thickness of the Indian shield is 40–44 km, as at Jabalpur, then beneath the 1 km high Shillong Plateau we believe it could reach 50–55 km, and that all of these earthquakes could have been in the lower continental crust. However, as Chen & Molnar (1990) pointed out, there is some residual uncertainty about whether the crust underlying the Bengal basin south of the plateau, and over which the Shillong Plateau is being thrust, is old (Cretaceous?) oceanic crust, rather than continental crust.

In a different category from the earthquakes discussed so far is a group that occurred at depths of 70–90 km beneath the Higher Himalaya and southern Tibet (Fig. 14). These earthquakes appear to be just beneath the Moho depth of 70–80 km determined by receiver functions (Kind *et al.* 1996) and therefore in the mantle. Various authors have argued that these are not in material originally attached to India and that has

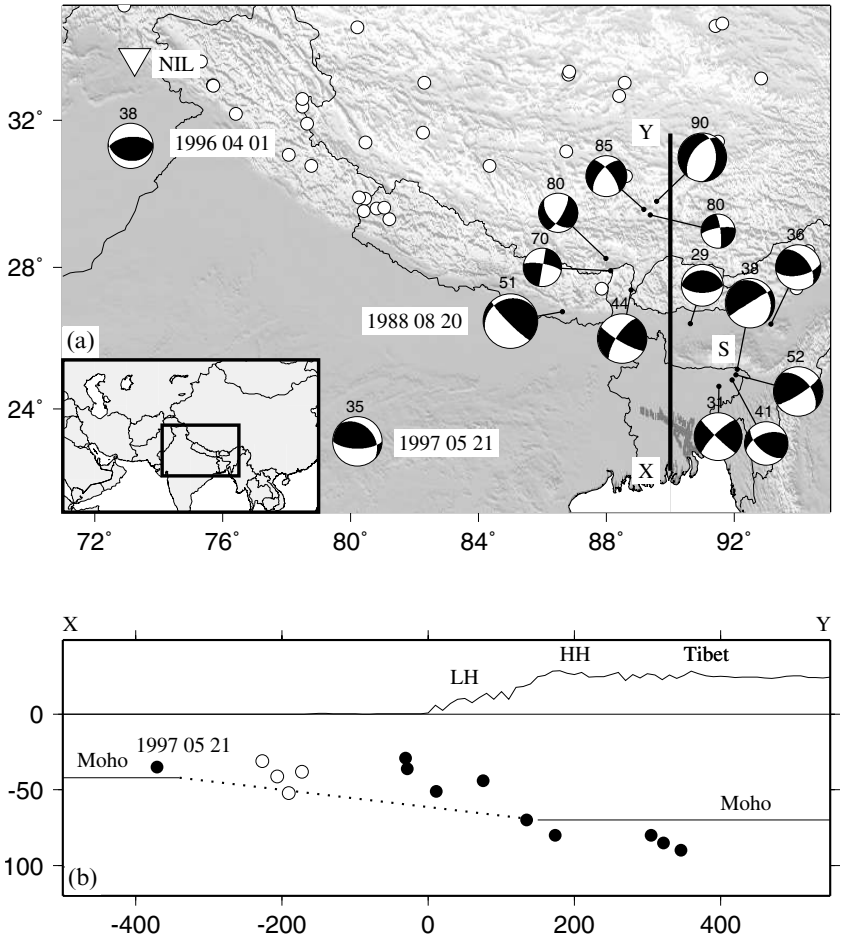

Figure 14. (a) Earthquakes with well-determined depths of 20 km or more in northern India, the central Himalayas and southern Tibet (Table 4). Numbers above the focal spheres refer to depths in km. Small circles are earthquakes whose depths of <20 km have also been well determined by the authors listed in Table 4. The white triangle represents the broad-band seismic station at Nilore (NIL). The Shillong Plateau is marked by S. X and Y mark the limits of the cross-section in (b). (b) Cross-section along 90°E showing the distribution of the deeper earthquakes in (a). LH marks the lesser Himalaya and HH the higher Himalaya. Events from the Shillong Plateau are marked by open circles. The depth of the Jabalpur earthquake of 1997.05.21, which is a long way west of the section, is marked to illustrate the depth of the probable Moho beneath the undeformed Indian shield (see text), and the 1996.04.01 event near Nilore is not shown. The Moho is shown to deepen from ~40 km south of the Ganges basin to reach a depth of ~70 km beneath Tibet and the high Himalaya (Kind *et al.* 1996), but whether it does so in the regular way indicated by the dotted line in unknown. The distances and depths on the cross-section are in km, and the elevation is exaggerated five times.

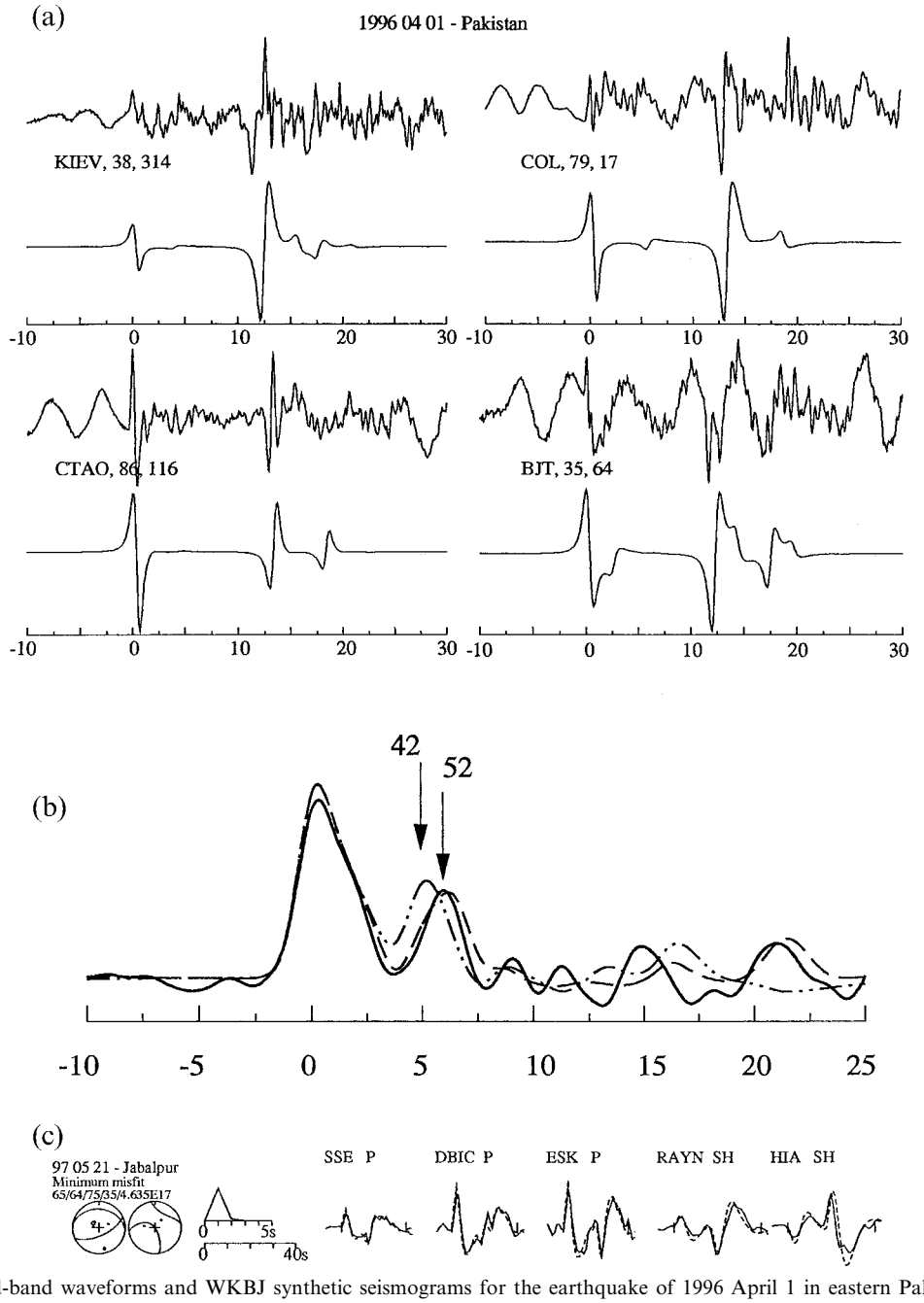

Figure 15. (a) Broad-band waveforms and WKBJ synthetic seismograms for the earthquake of 1996 April 1 in eastern Pakistan (see Fig. 14a). Synthetics were calculated using a depth of 38 km and a crustal velocity structure determined from the NIL receiver function in (b) below. The name of each station is followed by its distance and azimuth from the epicentre. (b) Receiver functions (Langston 1979) for the GDSN station at NIL. The solid line is the stacked receiver function formed from three earthquakes in the distance range 40°–45°. The dashed line is the synthetic receiver function for a crust 52 km thick, determined from inversion of the observed receiver function. The dot-dashed line is a synthetic receiver function calculated for a 42 km thick crust. The second prominent pulse is the *P*-to-*S* conversion at the Moho. From these observations we estimate the crustal thickness at NIL to be 52 ± 2 km. (c) Selected waveforms from the minimum-misfit inversion solution for the 1997 May 21 Jabalpur earthquake (see Fig. 14a). The display convention is the same as in Fig. 3, and the full solution is given in the Appendix.

underthrust Tibet, mainly because their focal mechanisms are neither those expected at intermediate depths in slabs nor low-angle thrusts, but instead they resemble the normal and strike-slip mechanisms seen at upper crustal depths in the same place (e.g. Chen *et al.* 1981; Chen & Kao 1996; Zhu & Helmberger 1996). Thus, one interpretation of these events is that they represent the response of the uppermost continental mantle to whatever is also deforming the upper continental crust, where focal depths are generally restricted to the top 15 km (Molnar & Lyon-Caen 1989). We are suspicious of this interpretation for three reasons: (1) these anomalously deep earthquakes are apparently restricted to this region of southern Tibet, whereas the shallow strike-slip and normal faulting is widespread; (2) their locations are close to an extrapolation of

the Indian shield northwards; and (3) there is the possibility that the Indian shield reaches this far north (e.g. Nelson *et al.* 1996) and exerts a basal traction that is transmitted throughout its overlying material (McCaffrey & Nabelek 1998). In short, while a case can be made for these earthquakes at 70–90 km being in the mantle, it is not clear to us that it has to be continental mantle originally beneath the Indian shield or Tibet rather than mantle belonging to a piece of originally oceanic lithosphere (a point made also by Chen & Molnar 1983).

To summarize, there is abundant evidence for lower crustal seismicity in the Indian shield, but no unequivocal evidence for seismicity in the continental mantle beneath that shield.

6 DISCUSSION

6.1 Bulletin and catalogue focal depth determinations

Our experience in the Zagros–Makran and Tien Shan shows that, although there is an undoubted general improvement in locations shown by the EHB catalogue over the ISC catalogue (see Engdahl *et al.* 1998), important errors in depth can still occur for shallow crustal earthquakes in some regions. Of the better-located depths (i.e. those labelled DEQ) reported as deeper than 30 km in the Zagros by the EHB catalogue and which were big enough for us to check with waveform analysis, none was deeper than 20 km, and we found discrepancies with the EHB depths as great as 40 km. Figs 16(a) and (c) compare the discrepancies between EHB depths and the centroids determined by body waves. There is a suggestion that the discrepancy decreases for genuinely deeper events, particularly for events deeper than about 60 km, and for larger events ($M_w > 5.5$). This effect is not surprising, given that the EHB depth determinations are based on reported high-frequency (~ 1 s) regional and teleseismic *P* and *S* phases, *PKP* phases, and the teleseismic depth phases *pP*, *pwP* and *sP*. At depths greater than ~ 50 km, when the *pP*–*P* time separation is ~ 15 s, the surface reflections are often clear and easily recognized, and source time functions are often simple and quite impulsive. At shallow depths, *pP* and *sP* can easily be misidentified on short-period records and confused with other phases arising from near-source structure, complicated source time functions or multiple subevents. For small-magnitude events in particular, waveforms at teleseismic distances may have small signal-to-noise ratios, making it hard to pick out the depth phases. The signal-to-noise ratios generally improve at regional distances, but here the often complex structure through which the seismic waves are propagating causes the seismograms themselves to be rather complex, which again makes finding and identifying depth phases rather difficult. Furthermore, in the absence of stations within the inflection point of the traveltime curve, EHB depth phase identifications can be highly dependent on the starting depth of the EHB location. When the EHB inversions were started at the depth we obtained from waveform modelling (E. R. Engdahl, personal communication, 2000), the discrepancies between the new EHB depths and our waveform depths were in all cases reduced to less than 20 km, as shown in Figs 16(b) and (d). There is little evidence for a correlation between depth discrepancy and either depth or magnitude for the new EHB depths (Figs 16c and d).

Our analysis of the 1985.02.02 (Section 3.3) and 1985.03.27 (Section 3.4) earthquakes in the Zagros suggests that serious

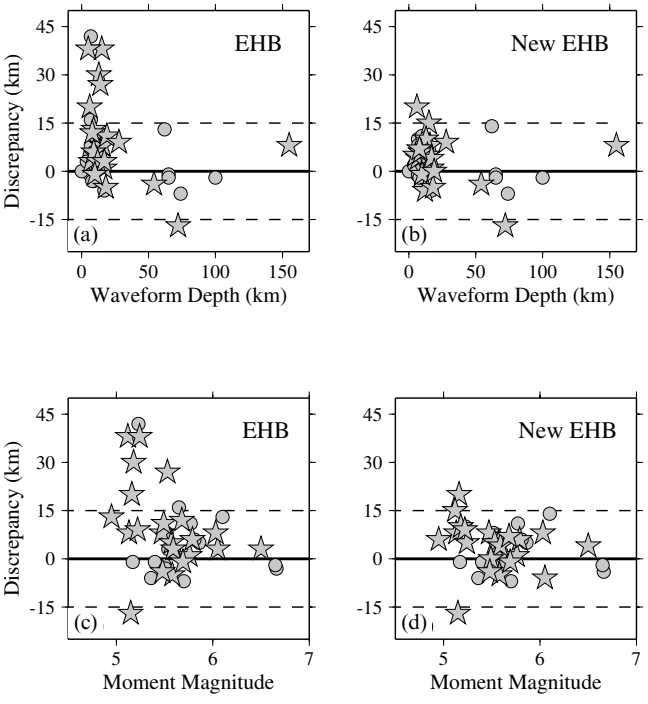

Figure 16. Comparison between the EHB depths and those obtained by waveform inversion in the Zagros–Makran. (a) Depth discrepancy (i.e. the EHB depth minus the waveform depth) against the depths determined by waveform analysis for all the events in Tables 1 and 2. (b) Discrepancy between the depths obtained by starting the EHB inversions at the waveform-determined depths and these same depths, plotted against depth. (c), (d) Depth discrepancies plotted against moment magnitude. Stars refer to events whose depths were determined in this study.

errors in depth and focal mechanism can also arise in long-period CMT determinations such as those published by Harvard. These solutions are determined using low-pass-filtered long-period body and mantle waveform data and the moment tensor inversion method described by Dziewonski *et al.* (1981). If the depth is not perturbed during the inversion, it is fixed to be consistent with the waveform matching of reconstructed broad-band body waves (Ekström 1989). Depths for most crustal earthquakes are poorly determined by the Harvard method and are usually fixed at an arbitrary, but sensible, depth of 15 km in the CMT catalogue. Table 1 also shows discrepancies in depth with those provided by the USGS. The USGS moment tensor inversions are based on long-period vertical-component *P* waveforms obtained from digital recording stations (Sipkin 1982, 1986a,b). The source depth that gives the smallest normalized mean-square error is a byproduct of the inversion, but for crustal earthquakes these depths are also poorly resolved.

It therefore seems clear to us that unverified catalogue depths are insufficiently accurate to resolve the relatively subtle differences in focal depth distribution within the crust that are of interest to us here. We conclude that in the Zagros, seismicity is confined to the upper 20 km of the crust whereas in the Tien Shan it occurs throughout a crustal thickness of 40 km. This contrast could not have been determined with confidence from bulletin or catalogue locations, nor, in particular, should unverified catalogue depths of 50–100 km be used as evidence for seismicity in the mantle lithosphere or for subduction.

6.2 Earthquakes in the continental mantle lithosphere?

Chen & Molnar (1983) concluded that in many regions of continental convergence the uppermost mantle is seismically active. It is worth examining how that evidence looks today, and for this purpose we ignore unverified depths reported by bulletins and catalogues based on arrival time data. In the Zagros, Tien Shan and Indian shield there is no unequivocal evidence for mantle seismicity. Certainly in the Tien Shan, Indian shield and parts of East Africa (Zhao *et al.* 1997; Foster & Jackson 1998) there are earthquakes whose waveform-determined centroids are very close to the Moho and, given the uncertainty in their depths and the crustal thickness, could have occurred in the uppermost mantle. However, they could just as well have occurred in the lower crust, which other earthquakes nearby show is definitely seismogenic in all three places. We would feel more confident about assigning seismicity to the continental mantle if there were earthquakes with depths definitely beneath the Moho, not just close to it on the crustal side. The remaining areas where Chen & Molnar (1983) suggested that seismicity in the continental mantle might occur split into two groups: those near places where subduction is occurring now or has occurred within the recent past, and those that have no plausible association with subduction.

The first group includes earthquakes at $\sim$100 km under the Karakoram in central Asia and the high Atlas in north Africa. As with the earthquakes at 70–90 km in southern Tibet that were discussed above, Chen & Molnar (1983) thought it unlikely that these occurred within downgoing slabs of lithosphere, mainly because their focal mechanisms do not fit into the usual pattern of P or T axes aligned down the dips of likely potential slabs, yet both the Karakoram and the Atlas are sites where oceanic lithosphere is very likely to have been subducted into the mantle in the late Tertiary. The problem then is in proving that these mantle events did not occur in lithosphere of oceanic origin (as Chen & Molnar 1983 pointed out).

The second group consists of isolated anomalies. Marks & Lindh (1978) reported two small (M_L1.1) events at depths of about 40 km beneath the foothills of the Sierra Nevada in California, where most seismicity is shallower than 20 km. In this region, which is one of present-day extension rather than shortening, the Moho depth is in the range 30–40 km (Spieth *et al.* 1981), so these earthquakes could conceivably be in the lowermost crust. In the Baikal region, Déverchère *et al.* (1991) found some microearthquakes at $\sim$40 km, but the rather large seismograph station spacing and lack of knowledge of Moho depths must cast doubt as to whether these were actually in the mantle. Assumpção & Suárez (1988) determined a focal depth of $\sim$45 km for an earthquake in the Brazilian shield near Manaus, in a region where the crustal thickness is unknown. Finally, Zandt & Richins (1979) reported a small (M_L3.8) isolated strike-slip earthquake at 90 ± 5 km in northern Utah, which must be in the mantle.

There is, of course, no doubt that in the oceanic lithosphere numerous intraplate earthquakes occur within the mantle (e.g. Chapple & Forsyth 1979; Wiens & Stein 1983). There are also other places, besides those discussed explicitly here, where seismicity occurs at depths greater than 20 km in the continental crust, and these are summarized in Table 5. However, the only earthquake we know of that must have occurred in the continental mantle is the small, isolated event at 90 km in Utah, mentioned above. We therefore conclude that there is no compelling evidence to believe that earthquakes in the uppermost mantle of the continental lithosphere are either common or an important indicator of mechanical strength.

Table 5. Summary of locations where earthquakes have been observed deeper than 20 km in the continental crust. The middle column refers to whether the depth determinations are from local or regional seismic networks or from teleseismic waveform analysis.

Location	Type of Analysis	Comments
Gazli, Uzbekistan	local	Earthquakes to 20–25 km ($\pm$3 km). Crustal thickness $\sim$40 km (Bossu *et al.* 1996).
Saguenay, Canada	teleseismic and local	Earthquakes, including one of M_w5.8, to $\sim$26 km. Crustal thickness $\sim$43 km (Somerville *et al.* 1990).
Crownpoint, NM	regional and local	Two events at 41 ± 7 km and 44 ± 4 km (regional). Aftershocks mostly at 22–32 km (local). Moho at 45–50 km (Wong *et al.* 1984).
Paradox Basin, UT	local	Seismicity generally to $\sim$40 km. Two isolated events at 53 and 58 km, but errors uncertain: probably $\pm$2–5 km, but may be $\pm$10 km. Moho at 45–50 km (Wong & Humphrey 1989).
Randolph, UT	local	Single event at 90 km, possible second at 55 km. Moho at $\sim$36 km (Zandt & Richins 1979; Zandt, personal communication, 1999).
Laramide Mts., WY	teleseismic	One event of m_b5.3 at 27.5 ± 1 km from modelling reconstituted broad-band waveform at RSNY. Moho at $\sim$41 km (Spence *et al.* 1996).
Ventura Basin, CA	local	39 small events between 20 and 30 km depth. Waveforms show depths are above the Moho at $\sim$32 km (Bryant & Jones 1989).
Sierra Foothills, CA	local	Many small events in the lower crust (Wong & Savage 1983).
Oroville, CA	local	Two small events at $\sim$40 km (Marks & Lindh 1978). Moho at 30–40 km (Spieth *et al.* 1981).
Southern Illinois	teleseismic and local	Earthquakes to 25 ± 3 km, including one of m_b5.5 (Chen & Molnar 1983; Chen 1988).
Manaus, Brazil	teleseismic	Earthquake of m_b4.1 at $\sim$45 km, confirmed by *pP* and *sP*, in Brazilian shield (Assumpção & Suárez 1988). Moho depth unknown.
East Africa (south)	teleseismic and local	Earthquakes of $m_b>5.5$ to $\sim$35 km depth (teleseismic). Smaller events in lower crust (local). Moho at 36–45 km in Proterozoic and Archaean shields (Zhao *et al.* 1997; Foster & Jackson 1998).
Oman Line (Iran)	teleseismic	Earthquake at $\sim$28 km (this paper, Section 3).
North India	teleseismic and local	Numerous events including $m_b>5.5$ in the lower crust (this paper, Section 5).
Tien Shan	teleseismic and regional	Numerous events including $m_b>5.5$ in the lower crust (this paper, Section 4).

6.3 Focal depth distributions and the rheology of the continental lithosphere

It remains true that most continental seismicity is concentrated in the upper crust. In many places, such as most of California (Hill *et al.* 1990), the Aegean (Taymaz *et al.* 1991), Tibet (Molnar & Lyon-Caen 1989) and the Zagros, seismicity is essentially confined to the upper 20 km of the crust and the lower crust is effectively aseismic. In other places (summarized in Table 5), including parts of East Africa (Zhao *et al.* 1997; Foster & Jackson 1998), the Tien Shan, the Indian shield and around Lake Baikal (Déverchère *et al.* 1991), lower crustal seismicity is more important, but is usually less intense than in the upper crust. The major modification since the reviews by Chen & Molnar (1983) and Chen (1988) is the reduced evidence for seismicity in the mantle beneath the continental lithosphere. As Chen (1988) pointed out, in several places there is an apparent concentration of seismicity at depths near the Moho, with mid-crustal levels apparently showing fewer earthquakes. However, it seems to us that the balance of evidence now favours the interpretation that these events occurred in the lower crust rather than in the upper mantle. These lower crustal events are evidently more common in old shield areas (see also Chen 1988).

These observations raise several questions. One is whether the places with thicker seismogenic crust, in which the lower crust is also seismically active, represent stronger continental lithosphere, and whether this can be recognized in the effective elastic thickness variations detected by methods such as that used by McKenzie & Fairhead (1997). Another is what causes such variations in seismogenic thickness within the continental crust, and particularly what can lead to the continental mantle being aseismic under shields whereas the oceanic mantle is clearly capable of producing earthquakes. These questions are beyond the scope of this paper, which has concentrated on seismological evidence, but are discussed in a separate study (Maggi *et al.* 2000). In brief, variations in the seismogenic thickness correlate with variations in the effective elastic thickness (T_e), which is usually the smaller of the two. Thus, T_e in the forelands of the northern Tien Shan and Himalaya is roughly 40 km, whereas it is only about 15–20 km around Iran. While the main control on rheological properties and strength is still likely to be homologous temperature, we believe the other important effect to be the presence (or absence) of volatiles, particularly water, small amounts of which are known to reduce strength dramatically (e.g. Mackwell *et al.* 1998). The young oceanic mantle is essentially dry, whereas the old continental mantle beneath shields slowly accumulates hydrous phases, formed by the crystallization of melts percolating upwards from the asthenosphere (McKenzie 1989; Harte *et al.* 1993). There may be sufficient water to reduce the strength of the old continental mantle but not of the younger oceanic mantle, which has accumulated less in the shorter time available. Similarly, it may be the loss of hydrous granitic melts from the deep continental crust, leaving anhydrous mafic granulites as residues, that is responsible for the increased strength and lower crustal seismicity in some old shield regions (Foster & Jackson 1998).

A final question concerns whether this variation in the thickness and strength of the continental seismogenic layer influences the scale of the structures that form within it. In particular, the seismogenic thickness seems to control the maximum segmentation length of the major dip-slip faults and the width of fault-bounded graben (e.g. Jackson & White 1989; Jackson & Blenkinsop 1997; Scholz & Contreras 1998; Ebinger *et al.* 1999). This question is further discussed by Maggi *et al.* (2000).

7 CONCLUSIONS

Most earthquakes in the continental lithosphere occur in the upper crust (typically <20 km depth) and in some regions, such as southern Iran, the Aegean, Tibet and most of California, they are virtually restricted to this depth. In other places, such as parts of East Africa, the Tien Shan and northern India, earthquakes occur throughout the continental crust to Moho depths as great as $\sim$40–45 km. These variations cannot be reliably detected from published bulletins or catalogues based on teleseismic arrival time data, even from those whose depth resolution is improved, such as the EHB catalogue of Engdahl *et al.* (1998). In the Zagros we found depth errors of up to 40 km in the EHB and Harvard CMT catalogues, and incidentally showed that two earthquakes with unusual CMT mechanisms showing normal faulting probably involved thrust faulting instead. Except for a single, small (M_L3.8), isolated event in Utah, we know of no compelling evidence that the continental mantle lithosphere is seismically active anywhere, although the oceanic mantle is certainly known to produce earthquakes. Thus there is little support in earthquake focal depth distributions for the idea that the uppermost mantle is significantly stronger than the lower crust in continental regions. The simplest interpretation of these observations is that the strength of the continental lithosphere resides in the crust and varies regionally, with an effective elastic thickness approximately corresponding to the seismogenic thickness.

ACKNOWLEDGMENTS

We are especially grateful to Dr E. R. Engdahl for a particularly generous, detailed and careful review that went far beyond the obligations of duty. Not only did he correct several errors and misconceptions in our assessment of the EHB catalogue, but he also carried out (and allowed us to quote) tests in which 'new EHB' locations in Figs 16(b) and (d) were determined in inversions using starting depths corresponding to those obtained from waveform modelling. His comments clarified our understanding of teleseismic depth determinations significantly, although we emphasize that we alone are responsible for any remaining misconceptions. We thank Dan McKenzie and Peter Molnar for helpful reviews, and W.-P. Chen for guiding us to some obscure literature. This is Cambridge Earth Sciences contribution ES 5939.

REFERENCES

Acharyya, S.K., Kayal, J.R., Roy, A. & Chaturvedi, R.K., 1998. Jabalpur earthquake of May 22, 1997: constraint from aftershock study, *J. geol. Soc. India,* **51,** 295–304.

Assumpção, M. & Suárez, G., 1988. Source mechanism of moderate-size earthquakes and stress orientation in mid-plate South America, *Geophys. J. Int.,* **92,** 253–267.

Baker, C., 1993. The active seismicity and tectonics of Iran, *PhD thesis,* University of Cambridge, Cambridge.

Baker, C., Jackson, J. & Priestley, K., 1993. Earthquakes on the Kazerun Line in the Zagros Mountains of Iran: strike-slip faulting within a fold-and-thrust belt, *Geophys. J. Int.,* **115,** 41–61.

Battacharya, S.N., Ghose, A.K., Suresh, G., Baidya, P.R. & Saxena, R.C., 1997. Source parameters of Jabalpur earthquake of 22 May 1997, *Current Sci.,* **73,** 855–863.

Bird, P., Toksöz, M. & Sleep, N., 1975. Thermal and mechanical models of continent-continent convergence zones, *J. geophys. Res.,* **80,** 4405–4416.

Bossu, R., Grasso, J.R., Plotnikova, L.M., Nurtaev, B., Frechet, J. & Moisy, M., 1996. Complexity of intracontinental seismic faultings: the Gazli, Uzbekistan, sequence, *Bull. seism. Soc. Am.,* **86,** 959–971.

Brace, W.F. & Byerlee, J.D., 1970. California earthquakes: why only shallow focus?, *Science,* **168,** 1573–1576.

Bryant, A.S. & Jones, L.M., 1989. Anomalously deep earthquakes in the crust beneath the Ventura basin, southern California, *EOS, Trans. Am. geophys. Un.,* **70,** 1209–1210.

Bump, H.A. & Sheehan, A.F., 1998. Crustal thickness variations across the northern Tien Shan from teleseismic receiver functions, *Geophys. Res. Lett.,* **25,** 1055–1058.

Byrne, D.E., Sykes, L.R. & Davis, D.M., 1992. Great thrust earthquakes and aseismic slip along the plate boundary of the Makran subduction zone, *J. geophys. Res.,* **97,** 449–478.

Chapman, C.H., 1978. A new method for computing synthetic seismograms, *Geophys. J. R. astr. Soc.,* **54,** 481–518.

Chapple, W.M. & Forsyth, D.W., 1979. Earthquakes and bending of plates at trenches, *J. geophys. Res.,* **84,** 6729–6749.

Chen, W.-P., 1988. A brief update on the focal depths of intra-continental earthquakes and their correlations with heat flow and tectonic age, *Seism. Res. Lett.,* **59,** 263–272.

Chen, W.-P. & Kao, H., 1996. Seismotectonics of Asia: some recent progress, in *The Tectonic Evolution of Asia,* pp. 37–62, eds Yin, A. & Harrison, M., Cambridge University Press, Palo Alto, CA.

Chen, W.-P. & Molnar, P., 1977. Seismic moments of major earthquakes and the average rate of slip in Central Asia, *J. geophys. Res.,* **82,** 2945–2969.

Chen, W.-P. & Molnar, P., 1983. Focal depths of intracontinental and intraplate earthquakes and their implications for the thermal and mechanical properties of the lithosphere, *J. geophys. Res.,* **88,** 4183–4214.

Chen, W.-P. & Molnar, P., 1990. Source parameters of earthquakes and intraplate deformation beneath the Shillong Plateau and northern Indoburman ranges, *J. geophys. Res.,* **95,** 12 527–12 552.

Chen, W.-P., Nabelek, J.L., Fitch, T.J. & Molnar, P., 1981. An intermediate depth earthquake beneath Tibet: source characteristics of the event of September 14, 1976, *J. geophys. Res.,* **86,** 2863–2876.

Déverchère, J., Houdry, F., Diament, M., Solonenko, N.V. & Solonenko, A.V., 1991. Evidence for a seismogenic upper mantle and lower crust in the Baikal rift, *Geophys. Res. Lett.,* **18,** 1099–1102.

Dziewonski, A.M., Chou, T.A. & Woodhouse, J.H., 1981. Determination of earthquake source parameters from waveform data for studies of global and regional seismicity, *J. geophys. Res.,* **86,** 2825–2852.

Ebinger, C., Jackson, J.A., Foster, A.N. & Hayward, N.J., 1999. Extensional basin geometry and the elastic lithosphere, *Phil. Trans. R. Soc. Lond.,* **A357,** 741–765.

Ekström, G.A., 1987. A broad band method of earthquake analysis, *PhD thesis,* Harvard University.

Ekström, G.A., 1989. A very broad-band inversion method for the recovery of earthquake source parameters, *Tectonophysics,* **166,** 73–100.

Engdahl, E.R., van der Hilst, R. & Buland, R., 1998. Global teleseismic earthquake relocation with improved travel times and procedures for depth determination, *Bull. seism. Soc. Am.,* **88,** 722–743.

Fan, G., Ni, J.F. & Wallace, T., 1994. Active tectonics of the Pamirs and Karakorum, *J. geophys. Res.,* **99,** 7131–7160.

Foster, A.N & Jackson, J.A., 1998. Source parameters of large African earthquakes: implications for crustal rheology and regional kinematics, *Geophys. J. Int.,* **134,** 422–448.

Ghose, S., Hamburger, M.W. & Ammon, C.J., 1998. Source parameters of moderate-sized earthquakes in the Tien Shan, central Asia, from regional moment tensor inversion, *Geophys. Res. Lett.,* **25,** 3181–3184.

Harte, B., Hunter, R.H. & Kinny, P.D., 1993. Melt geometry, movement and crystallization, in relation to mantle dykes, veins and metasomatism, *Phil. Trans. R. Soc. Lond.,* **A342,** 1–21.

Hill, D.P., Eaton, J.P. & Jones, L.M., 1990. Seismicity, 1980–86, in *The San Andreas Fault system, California,* ed. Wallace, R.E., *USGS. Prof. Pap.,* **1515,** 115–151.

Jackson, J., 1980. Errors in focal depth determination and the depth of seismicity in Iran and Turkey, *Geophys. J. R. astr. Soc.,* **61,** 285–301.

Jackson, J.A. & Blenkinsop, T., 1997. The Bilila-Mtakataka fault in Malawi: an active 100-km long, normal fault segment in thick seismogenic crust, *Tectonics,* **16,** 137–150.

Jackson, J. & Fitch, T., 1981. Basement faulting and the focal depths of the larger earthquakes in the Zagros mountains (Iran), *Geophys. J. R. astr. Soc.,* **64,** 561–586.

Jackson, J.A. & McKenzie, D.P., 1984. Active tectonics of the Alpine-Himalayan belt between western Turkey and Pakistan, *Geophys. J. R. astr. Soc.,* **77,** 185–264.

Jackson, J.A. & White, N.J., 1989. Normal faulting in the upper continental crust: observations from regions of active extension, *J. struct. Geol.,* **11,** 15–36.

Jacob, K. & Quittmeyer, R.C., 1979. The Makran region of Pakistan and Iran: trench-arc system with active plate subduction, in *Geodynamics of Pakistan,* pp. 305–317, eds Farah, A. & DeJong, K.A., Geological Survey of Pakistan, Quetta.

Kayal, J.R. & Zhao, D., 1998. Three-dimensional seismic structure beneath Shillong Plateau and Assam Valley, northeast India, *Bull. seism. Soc. Am.,* **88,** 667–676.

Kennett, B.L.N., Engdahl, E.R. & Buland, R., 1995. Constraints on seismic velocities in the Earth from travel times, *Geophys. J. R. astr. Soc.,* **122,** 108–124.

Kind, R., *et al.*, 1996. Evidence from earthquake data for a partially molten crustal layer in southern Tibet, *Science,* **274,** 1692–1694.

Kosarev, G.L., Petersen, N.V., Vinnik, L.P. & Roecker, S.W., 1993. Receiver functions for the Tien Shan analog broadband network: contrasts in the evolution of structures across the Talasso–Fergana Fault, *J. geophys. Res.,* **98,** 4437–4448.

Laana, J.L. & Chen, W.-P, 1989. The Makran earthquake of 1983 April 18: a possible analogue to the Puget Sound earthquake of 1965?, *Geophys. J. Int.,* **98,** 1–9.

Langston, C.A., 1979. Structure under Mt. Rainier, Washington, inferred from teleseismic body waves, *J. geophys. Res.,* **84,** 4749–4762.

Lemoine, F.G., *et al.*, 1996. The NASA and DMA joint geo-potential model, *EOS, Trans. Am. geophys. Un.,* **77,** Fall mtng suppl., F136.

Lyon-Caen, H. & Molnar, P., 1983. Constraints on the structure of the Himalaya from an analysis of gravity anomalies and a flexural model of the lithosphere, *J. geophys. Res.,* **88,** 8171–8191.

Mackwell, S.J., Zimmerman, M.E. & Kohlstedt, D.L., 1998. High-temperature deformation of dry diabase with application to tectonics on Venus, *J. geophys. Res.,* **103,** 975–984.

Maggi, A., Jackson, J.A., Mckenzie, D. & Priestley, K., 2000. Earthquake focal depths, effective elastic thickness, and the strength of the continental lithosphere, *Geology,* **28,** 495–498.

Mangino, S., Priestley, K. & Ebel, J., 1999. The receiver structure beneath the China digital seismograph network stations, *Bull. seism. Soc. Am.,* **89,** 1053–1076.

Marks, S.M. & Lindh, A.G., 1978. Regional seismicity of the Sierran foothills in the vicinity of Oroville, California, *Bull. seism. Soc. Am.,* **68,** 1103–1115.

McCaffrey, R. & Abers, J., 1988. SYN3: A program for inversion of teleseismic body wave form on microcomputers, *Air Force geophys. Lab. Tech. Rept,* **AFGL-TR-88-0099,** Hanscomb Air Force Base, Massachusetts.

McCaffrey, R. & Nábelek, J., 1987. Earthquakes, gravity, and the origin of the Bali Basin: an example of a nascent continental fold-and-thrust belt, *J. geophys. Res.,* **92,** 441–460.

McCaffrey, R. & Nabelek, J., 1998. Role of oblique convergence in the active deformation of the Himalayas and southern Tibet plateau, *Geology,* **26,** 691–694.
McKenzie, D., 1989. Some remarks on the movement of small melt fractions in the mantle, *Earth planet. Sci. Lett.,* **95,** 53–72.
McKenzie, D. & Fairhead, D., 1997. Estimates of the effective elastic thickness of the continental lithosphere from Bouguer and free air gravity anomalies, *J. geophys. Res.,* **102,** 27 523–27 552.
Molnar, P. & Chen, W.-P., 1983. Focal depths and fault plane solutions of earthquakes under the Tibetan plateau, *J. geophys. Res.,* **88,** 1180–1196.
Molnar, P. & Lyon-Caen, H., 1989. Fault plane solutions of earthquakes and active tectonics of the Tibetan plateau and its margins, *Geophys. J. Int.,* **99,** 123–153.
Moores, E.M. & Twiss, R.J., 1995. *Tectonics,* W. H. Freeman, New York.
Murty, A.S.N., Mall, D.M., Murty, P.R.K. & Reddy, P.R., 1998. Two-dimensional crustal velocity structure along Hirapur-Mandla profile from seismic refraction and wide-angle reflection data, *Pure appl. Geophys.,* **152,** 247–266.
Nelson, K.D., *et al.*, 1996. Partially molten middle crust beneath southern Tibet: synthesis of project INDEPTH results, *Science,* **274,** 1684–1688.
Nelson, M.R., McCaffrey, R. & Molnar, R., 1987. Source parameters for 11 earthquakes in the Tien Shan, Central Asia, determined by P and SH waveform inversion, *J. geophys. Res.,* **92,** 12 629–12 648.
Ni, J. & Barazangi, M., 1986. Seismotectonics of Zagros continental collision zone and a comparison with the Himalayas, *J. geophys. Res.,* **91,** 8205–8218.
Nowroozi, A.A., 1971. Seismotectonics of the Persian plateau, eastern Turkey, Caucasus, and Hindu Kush regions, *Bull. seism. Soc. Am.,* **61,** 317–341.
Nyblade, A.A. & Langston, C.A., 1995. East African earthquakes below 20 km depth and their implications for crustal structure, *Geophys. J. Int.,* **121,** 49–62.
Pegler, G. & Das, S., 1998. An enhanced image of the Pamir-Hindu Kush seismic zone from relocated earthquake hypocentres, *Geophys. J. Int.,* **134,** 573–595.
Priestley, K., Baker, C. & Jackson, J., 1994. Implications of earthquake focal mechanism data for the active tectonics of the south Caspian basin and surrounding regions, *Geophys. J. Int.,* **118,** 111–141.
Roecker, S.W., *et al.*, 1993. Three–dimensional elastic wave velocity structure of the western and central Tien Shan, *J. geophys. Res.,* **98,** 15 779–15 795.
Scholz, C.H. & Contreras, J.C., 1998. Mechanics of continental rift architecture, *Geology,* **26,** 967–970.
Sipkin, S.A., 1982. Estimation of earthquake source parameters by the inversion of waveform data, synthetic seismograms, *Phys. Earth planet. Inter.,* **30,** 242–259.
Sipkin, S.A., 1986a. Interpretation of non-double-couple earthquake source mechanisms derived from moment tensor inversion, *J. geophys. Res.,* **91,** 531–547.
Sipkin, S.A., 1986b. Estimation of earthquake source parameters by the inversion of waveform data: global seismicity, 1981–1983, *Bull. seism. Soc. Am.,* **76,** 1515–1541.
Somerville, P., McLaren, J.P., Saikia, C.K. & Helmberger, D.V., 1990. The 25 November 1988 Saguenay, Quebec, earthquake: source parameters and the attenuation of strong ground motion, *Bull. seism. Soc. Am.,* **80,** 1118–1143.
Spence, W., Langer, C.J. & Choy, G.L., 1996. Rare, large earthquakes at the Laramide deformation front—Colorado (1882) and Wyoming (1984), *Bull. seism. Soc. Am.,* **86,** 1804–1819.
Spieth, M.A., Hill, D.P. & Geller, R.J., 1981. Crustal structure in the northwestern foothills of the Sierra Nevada from seismic refraction experiments, *Bull. seism. Soc. Am.,* **71,** 1075–1087.
Taymaz, T., Jackson, J. & McKenzie, D., 1991. Active tectonics of the north and central Aegean Sea, *Geophys. J. Int.,* **106,** 433–490.
Wiens, D.A. & Stein, S., 1983. Age dependence of intraplate seismicity and implications for lithospheric evolution, *J. geophys. Res.,* **88,** 6455–6468.
Wong, I.G. & Humphrey, J.R., 1989. Contemporary seismicity, faulting and the state of stress in the Colorado plateau, *Geol. Soc. Am. Bull.,* **101,** 1127–1146.
Wong, I.G. & Savage, W.U., 1983. Deep intraplate seismicity in the western Sierra Nevada, central California, *Bull. seism. Soc. Am.,* **73,** 797–812.
Wong, I.G., Cash, D. & Jaksha, L., 1984. The Crowpoint, New Mexico, earthquakes of 1976 and 1977, *Bull. seism. Soc. Am.,* **74,** 2435–2449.
Zandt, G. & Richins, W.D., 1979. An upper mantle earthquake beneath the middle Rocky mountains in NE Utah, *Earthq. Notes,* **50,** 69–70 (abstract).
Zhao, M., Langston, C.A., Nyblade, A.A. & Owens, T.J., 1997. Lower-crustal rifting in the Rukwa graben, east Africa, *Geophys. J. Int.,* **129,** 412–420.
Zhu, L.P. & Helmberger, D.V., 1996. Intermediate depth earthquakes beneath the India-Tibet collision, *Geophys. Res. Lett.,* **23,** 435–438.
Zhu, L., Helmberger, D.V., Saikia, C.K. & Woods, B.B., 1997. Regional waveform calibration in the Pamir–Hindu Kush region, *J. geophys. Res.,* **102,** 22 799–22 813.

APPENDIX A: FULL-WAVEFORM INVERSION SOLUTIONS

This appendix contains the minimum-misfit *P* and *SH* waveforms (Figs A1–A14) for the 14 'a' class earthquakes in Table 1 not already discussed in the text, and also for the Jabalpur earthquake (Table 4) (Fig. A15). We used long-period *P* and *SH* waveforms to constrain the earthquake source parameters. The data is in the form of digital broad-band records from stations of the GDSN, which we transformed to records with the WWSSN long-period response. Where broad-band data were not available, we used the original long-period digital data. Onset arrival times were measured either from the original broad-band data or from short-period records. Inversions were performed using the MT5 version of McCaffrey & Abers' (1988) algorithm, which inverts *P* and *SH* waveform data to obtain the strike, dip, rake, centroid depth, seismic moment and source time function. The synthetic seismograms are formed by the addition of direct *P* or *SH* waves with the surface reflections *pP*, *sP* and *sS* and near-source multiples. Amplitudes are corrected for geometrical spreading, and for anelastic attenuation using a Futterman Q operator with a value for $t^{\star}$ of 1.0 s for *P* and 4.0 s for *SH* waves. We used *P* waveforms in the distance range 30°–90° and *SH* waves in the range 30°–75°. Uncertainties in the earthquake focal parameters were estimated according to the procedure described in Section 2.1 of the main text.

Each figure is divided into two parts. (a) The minimum-misfit solution panel, in which the values beneath the event header give strike, dip, rake, depth in kilometres and seismic moment in Newton metres. The upper circle shows the *P*-wave radiation pattern and the lower circle that for *SH*. Both are lower-hemisphere projections. The station code by each waveform is accompanied by a letter corresponding to its position on the focal sphere. These are ordered clockwise by azimuth. The solid lines are the observed waveforms and the dashed lines are the synthetic waveforms. The inversion window is marked by solid

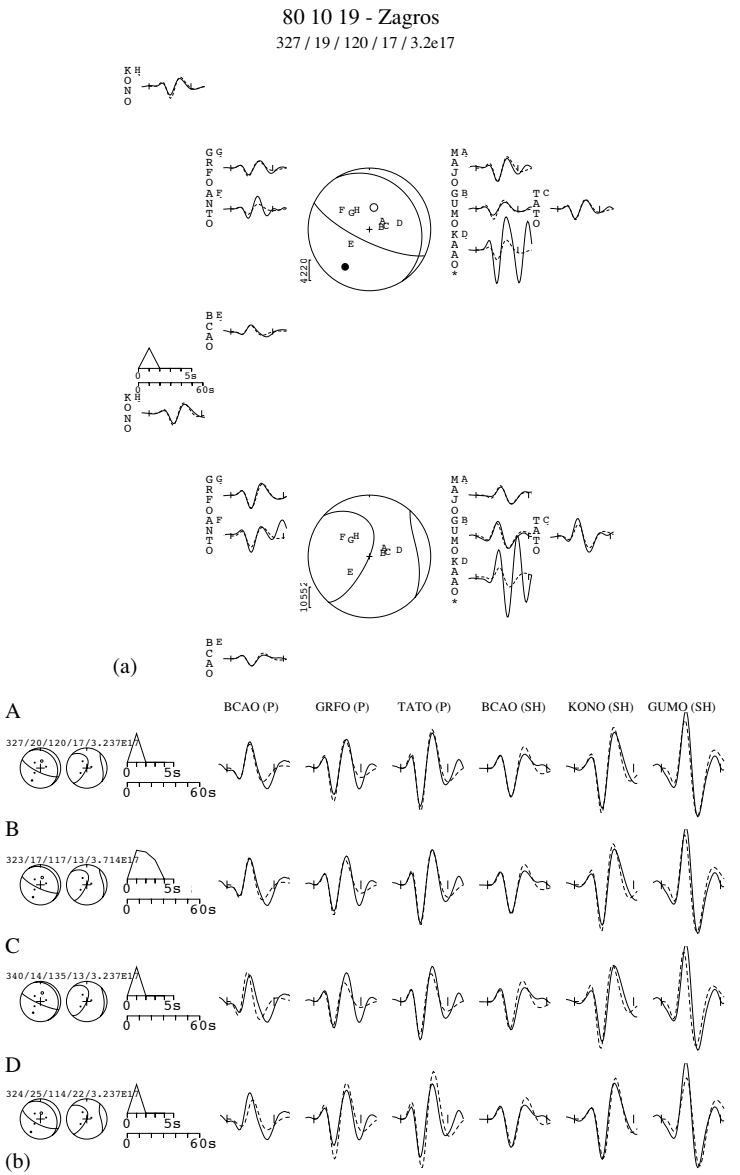

Figure A1. Zagros, 1980 October 19. (a) Minimum-misfit solution: strike 327°, dip 19°, rake 120°, depth 17 km, M_w5.6. The records at KAAO (indicated by *) were not used in the inversion procedure. (b) Sensitivity analysis. A: minimum-misfit solution shown in (a). B: depth fixed at 13 km; the source time function has doubled in length to fit the width of the first pulse. C: depth fixed at 13 km, source time function fixed to its value in A; the width of the first pulse is no longer matched. D: depth fixed at 22 km; the synthetic pulse is too wide. Event depth: 17^{+5}_{-4} km.

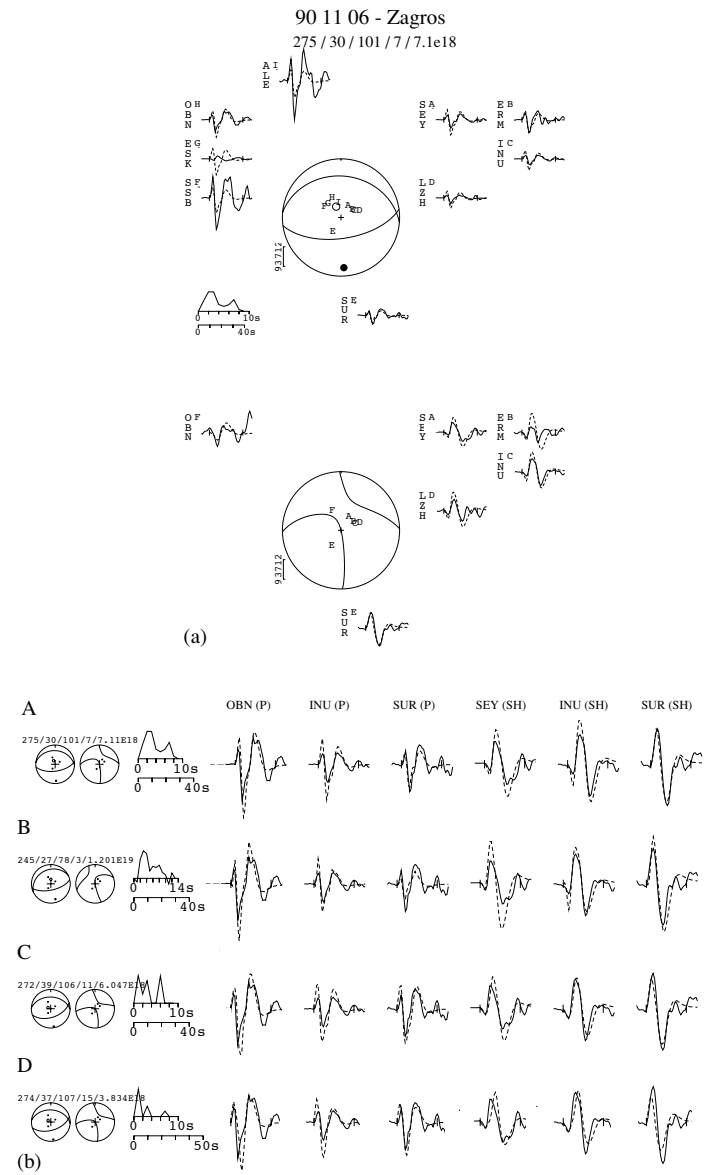

Figure A2. Zagros, 1990 November 6. (a) Minimum-misfit solution: strike 275°, dip 30°, rake 101°, depth 7 km, M_w6.5. (b) Sensitivity analysis. A: minimum-misfit solution shown in (a). B: depth fixed at 3 km; the source time function has expanded from 10 to 14 s duration and has become more complex. C: depth fixed at 11 km; the synthetic pulse is too wide. Event depth: 7 ± 4 km. D: the Harvard CMT solution (strike 274°, dip 37°, rake 107°, depth 15 km); the mechanism is similar to the minimum-misfit solution, but the synthetic waveforms are too broad.

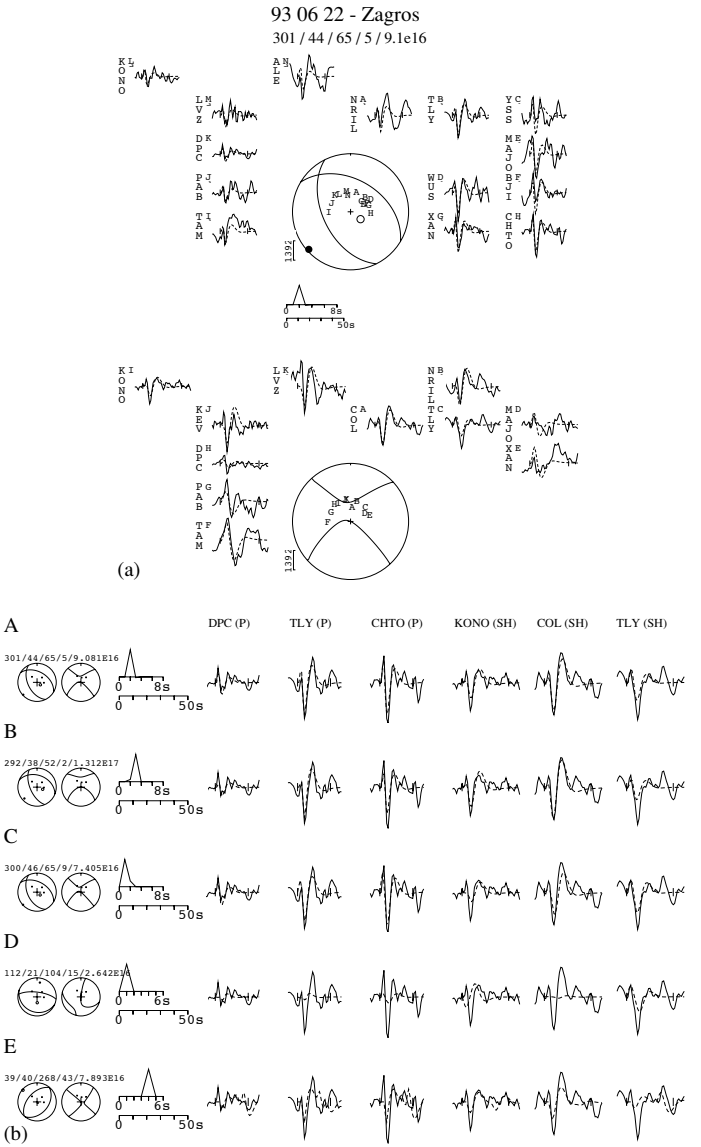

Figure A3. Zagros, 1993 June 22. (a) Minimum-misfit solution: strike 301°, dip 44°, rake 65°, depth 5 km, M_w5.2. (b) Sensitivity analysis. A: minimum-misfit solution shown in (a). B: depth fixed at 2 km; the fit is starting to deteriorate at TLY (*SH*). C: depth fixed at 9 km; the pulse is too broad at COL (*SH*). Event depth: 5^{+4}_{-3} km. D: the Harvard CMT solution (strike 112°, dip 21°, rake 104°, depth 15 km); the stations which should be nodal with this mechanism have non–nodal waveforms. E: best-fit mechanism for a depth fixed at the EHB depth (44 km); the first-motion polarities are now incorrect (showing a normal mechanism perpendicular to the strike of the region).

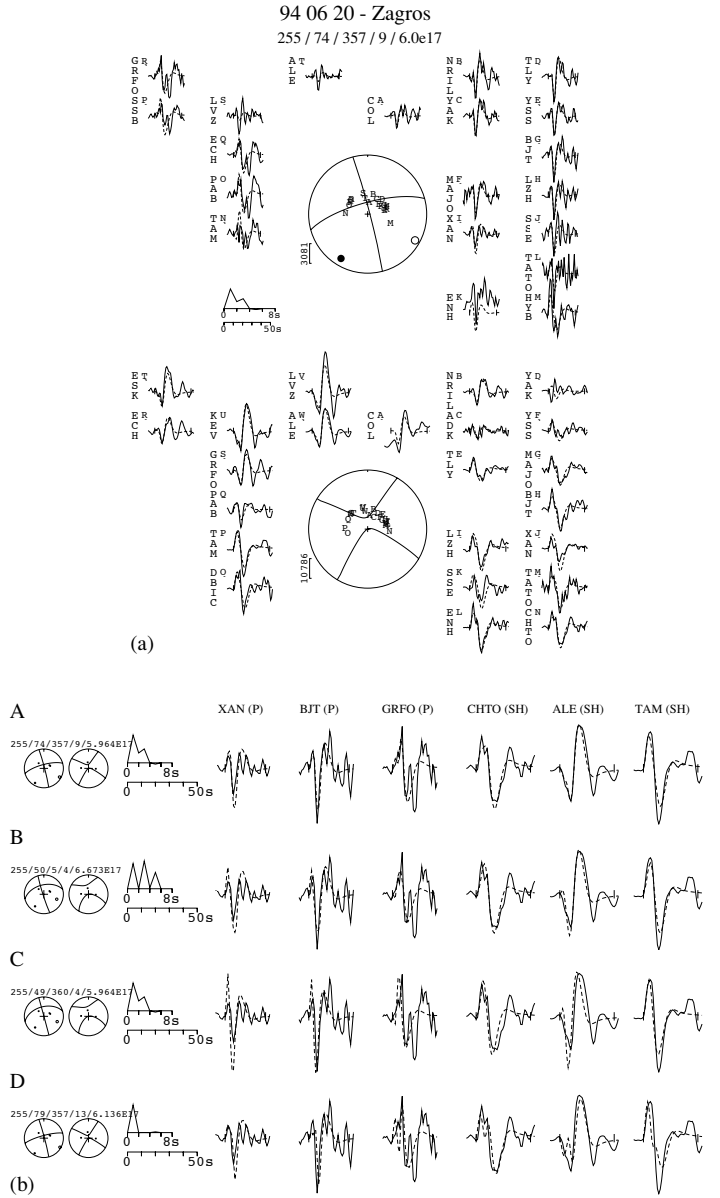

Figure A4. Zagros, 1994 June 20. (a) Minimum-misfit solution: strike 255°, dip 74°, rake 357°, depth 9 km, M_w5.8. (b) Sensitivity analysis. A: minimum-misfit solution shown in (a). B: depth fixed at 4 km; the source time function now shows three pulses. C: depth fixed at 4 km, source time function fixed to value in A; the synthetic waveforms are too narrow. D: depth fixed at 13 km; the synthetics are too broad. Event depth: 9^{+4}_{-5} km.

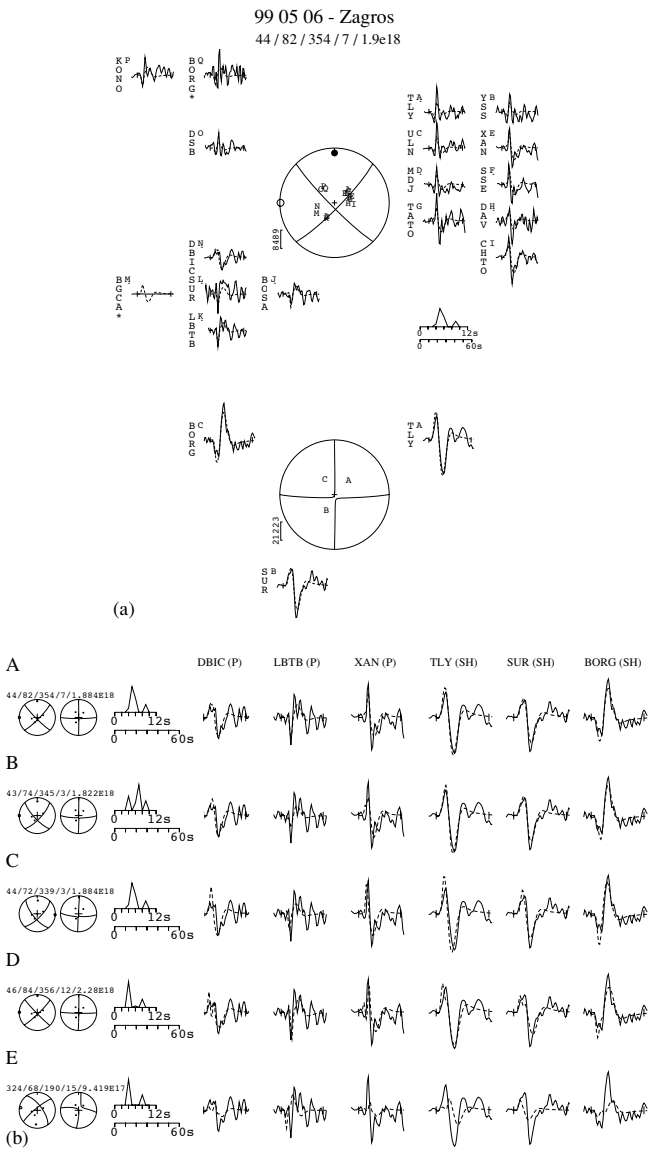

Figure A5. Zagros, 1999 May 6. (a) Minimum-misfit solution: strike 44°, dip 82°, rake 354°, depth 7 km, M_w6.1. The *P*-wave records at BGCA and BORG (indicated by *) were not used in the inversion. (b) Sensitivity analysis. A: minimum-misfit solution shown in (a). B: depth fixed at 3 km; the source time function shows three pulses. C: depth fixed at 3 km, source time function fixed to value in A; the synthetics are too narrow. D: depth fixed at 12 km; the synthetics are too broad. Event depth: 7^{+5}_{-4} km. E: the Harvard CMT solution (strike 324°, dip 68°, rake 190°, depth 17 km); the fit to the *SH* waveforms has deteriorated.

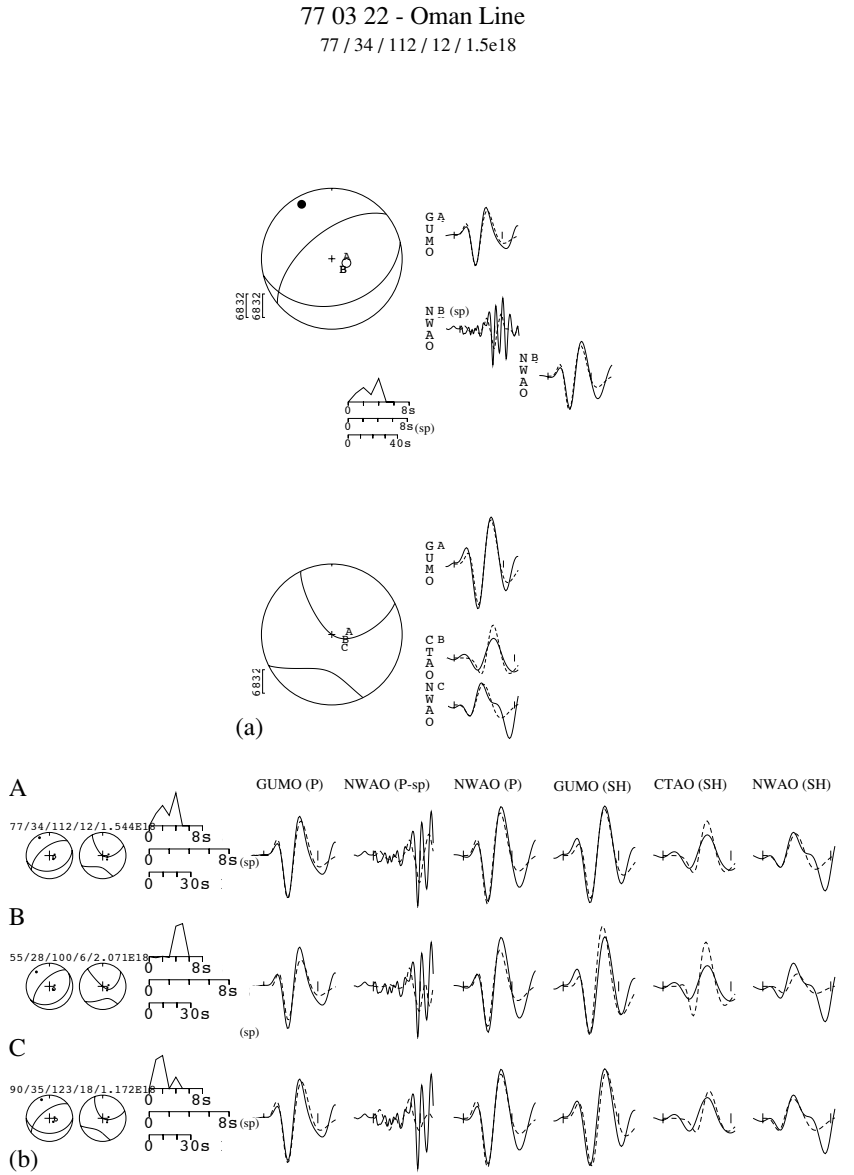

Figure A6. Oman Line, 1977 March 22. (a) Minimum-misfit solution: strike 77°, dip 34°, rake 112°, depth 12 km, M_w6.0. A short-period record at NWAO was included in the inversion. Although few stations were available, the focal mechanism is well constrained by the *SH* waves. (b) Sensitivity analysis. A: minimum-misfit solution shown in (a). B: depth fixed at 6 km; the synthetic pulse is too narrow at GUMO (*SH*), and its amplitude is too large at CTAO (*SH*). C: depth fixed at 18 km; the synthetic waveform is too broad at GUMO. Event depth: 12 ± 6 km.

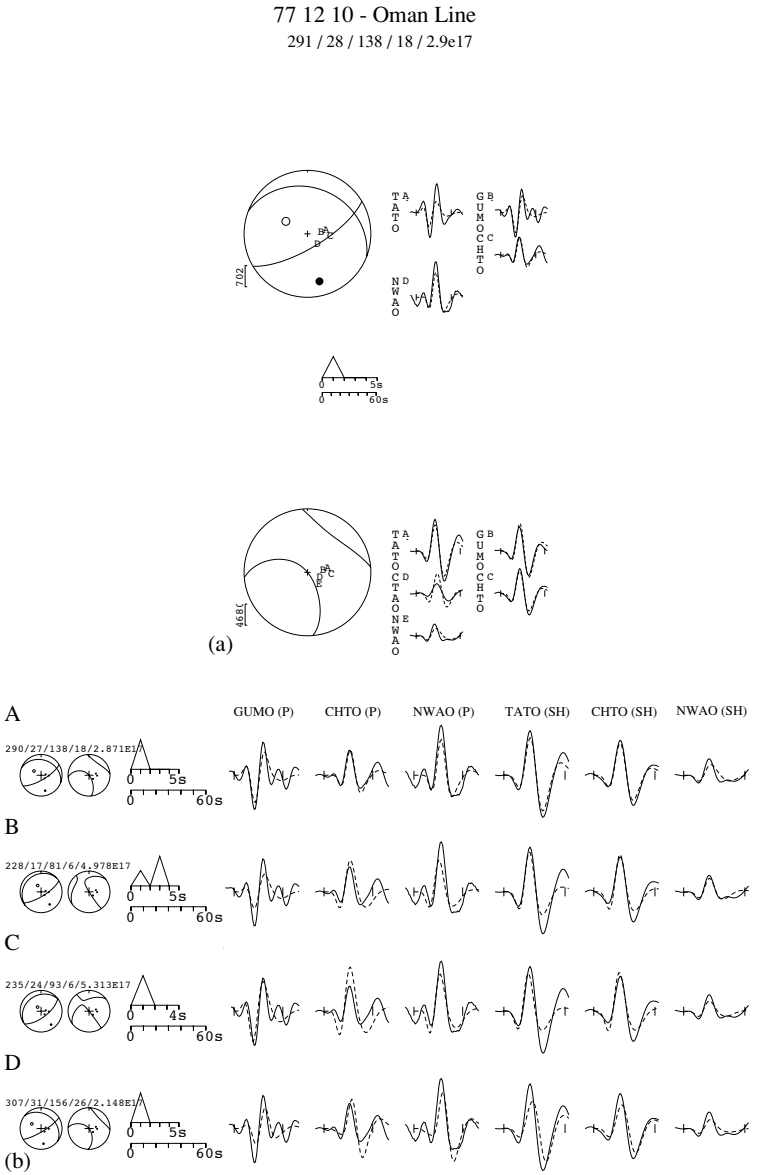

Figure A7. Oman Line, 1977 December 10. (a) Minimum-misfit solution: strike 291°, dip 28°, rake 138°, depth 18 km, M_w5.6. (b) Sensitivity analysis. A: minimum-misfit solution shown in (a). B: depth fixed at 6 km; the source time function has doubled in length. C: depth fixed at 6 km, source time function fixed to its value in A; the synthetics are too narrow, and the amplitude at CHTO (*P*) is too large. D: depth fixed at 26 km; the synthetics are too broad. Event depth: 18^{+8}_{-12} km.

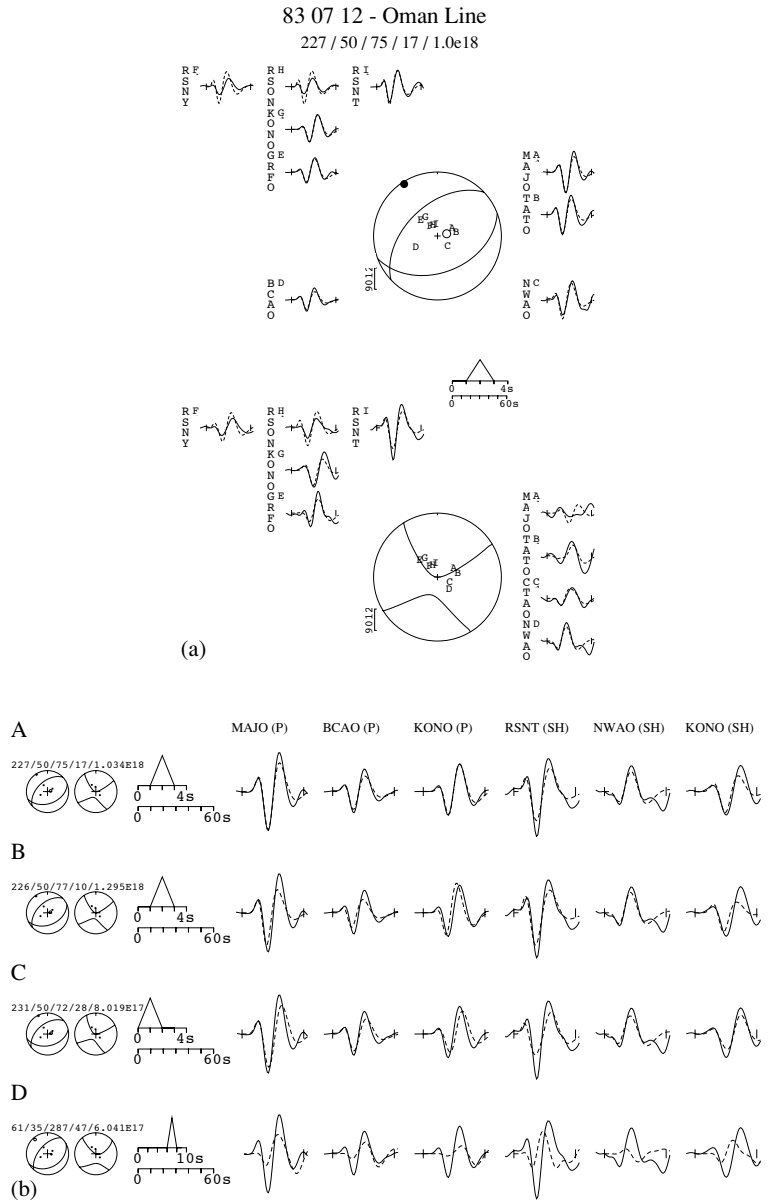

Figure A8. Oman Line, 1983 July 12. (a) Minimum-misfit solution: strike 227°, dip 50°, rake 75°, depth 17 km, M_w5.9. (b) Sensitivity analysis. A: minimum-misfit solution shown in (a). B: depth fixed at 10 km; the synthetics are too narrow. C: depth fixed at 28 km; the synthetics are too broad. Event depth: 17^{+11}_{-7} km. D: the Harvard CMT solution (strike 61°, dip 35°, rake 287°, depth 47 km); the fit has deteriorated at all stations.

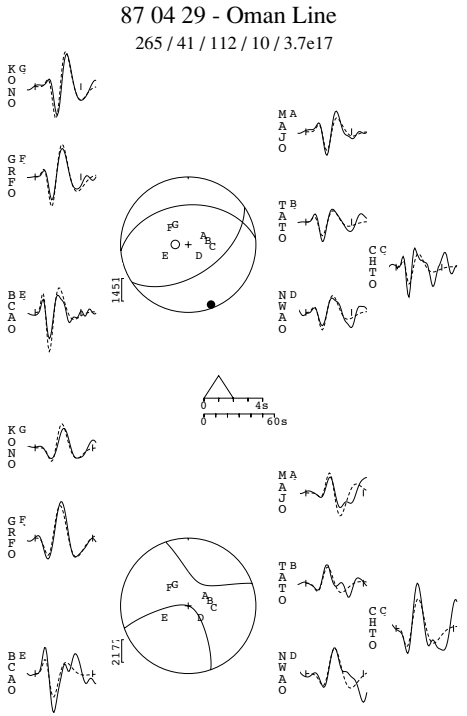

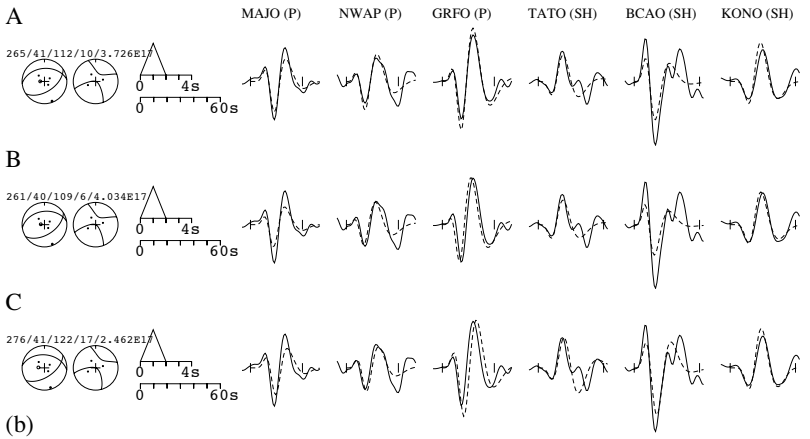

Figure A9. Oman Line, 1987 April 29. (a) Minimum-misfit solution: strike 265°, dip 41°, rake 112°, depth 10 km, M_w5.6. (b) Sensitivity analysis. A: minimum-misfit solution shown in (a). B: depth fixed at 6 km; the synthetic pulse is too narrow at GRFO (*P*) and its amplitude is too small at BCAO (*SH*). C: depth fixed at 17 km; the synthetics are too broad. Event depth: $10^{+7}_{-}4$ km.

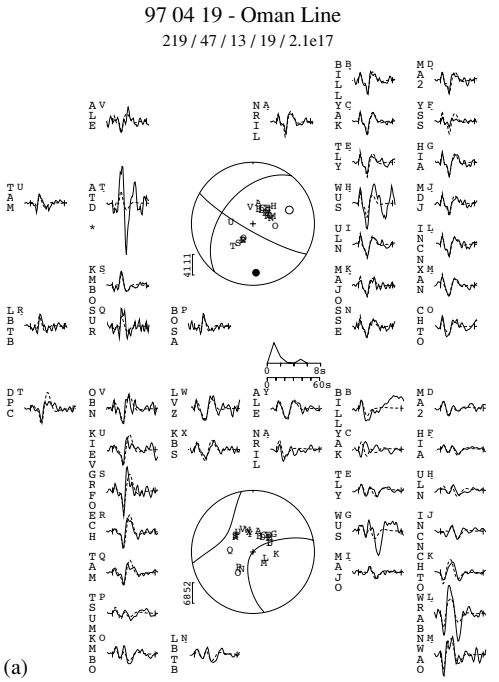

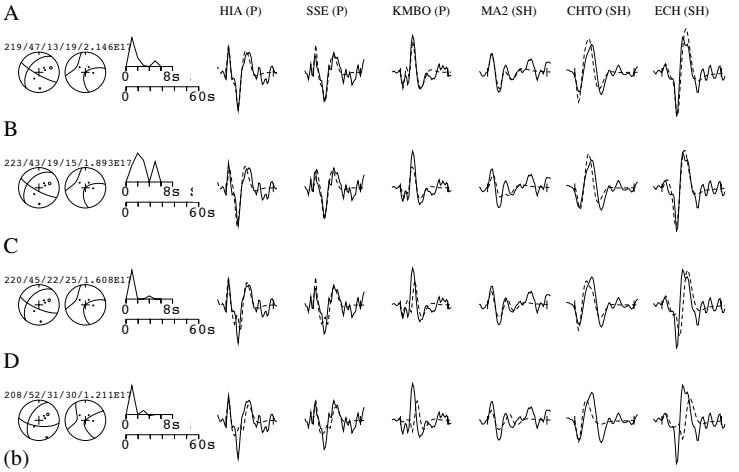

Figure A10. Oman Line, 1997 April 19. (a) Minimum-misfit solution: strike 219°, dip 47°, rake 13°, depth 19 km, M_w5.5. The *P*-wave record at ATD (indicated by *) was not used in the inversion. (b) Sensitivity analysis. A: minimum-misfit solution shown in (a). B: depth fixed at 15 km; the synthetic pulse is too narrow at CHTO (*SH*). C: depth fixed at 25 km; the synthetics are too broad. Event depth: $19^{+6}_{-}4$ km. D: depth fixed at the EHB value (30 km); the synthetics are too broad to fit the data.

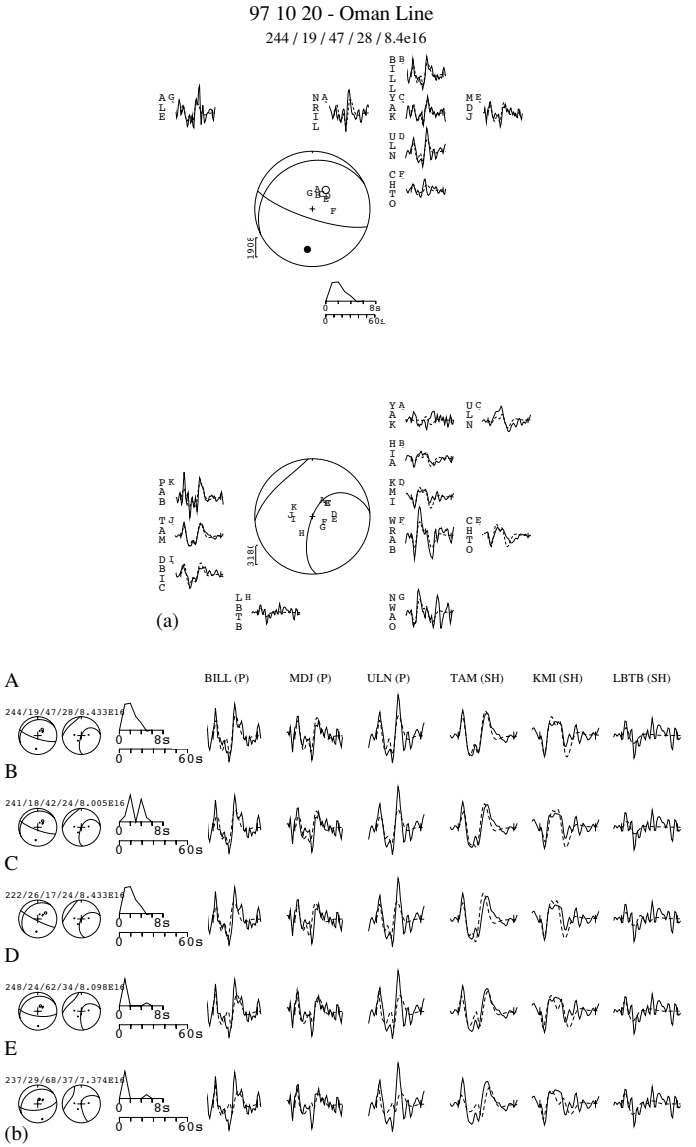

Figure A11. Oman Line, 1997 October 20. (a) Minimum-misfit solution: strike 244°, dip 19°, rake 47°, depth 28 km, M_w5.2. (b) Sensitivity analysis. A: minimum-misfit solution shown in (a). B: depth fixed at 24 km; the source time function has two peaks. C: depth fixed at 24 km, source time function fixed to its value in A; the synthetics are too narrow. D: depth fixed at 34 km; the fit has deteriorated at ULN (*P*) and TAM (*SH*). Event depth: 28^{+6}_{-4} km. E: depth fixed at the EHB value (37 km); the synthetics at BILL (*P*) and MDJ (*P*) no longer have the second trough, and those at ULN (*P*) and TAM (*SH*) are too broad.

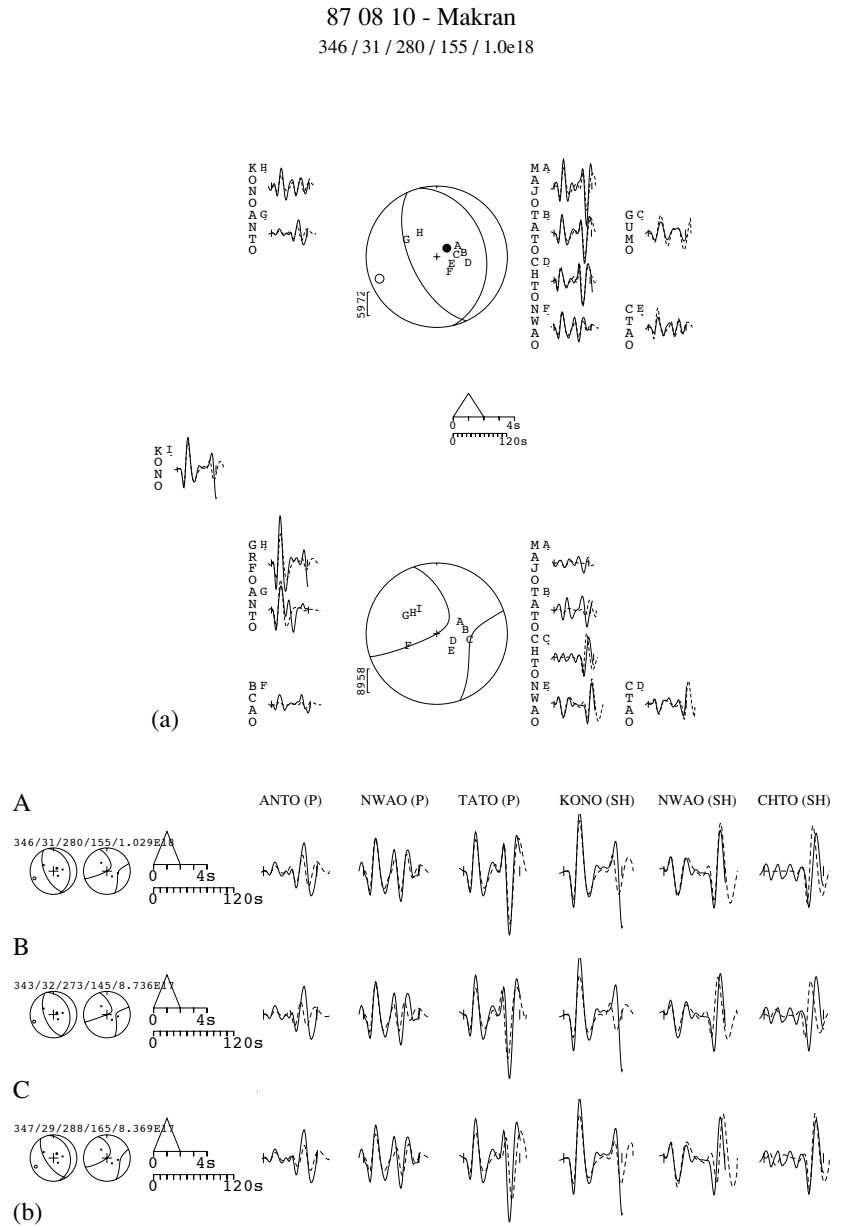

Figure A12. Makran, 1987 August 10. (a) Minimum-misfit solution: strike 346°, dip 31°, rake 280°, depth 155 km, M_w5.9. (b) Sensitivity analysis. A: minimum-misfit solution shown in (a). B: depth fixed at 145 km; the synthetics are too narrow. C: depth fixed at 165 km; the synthetics are too broad. Event depth: 155 ± 10 km.

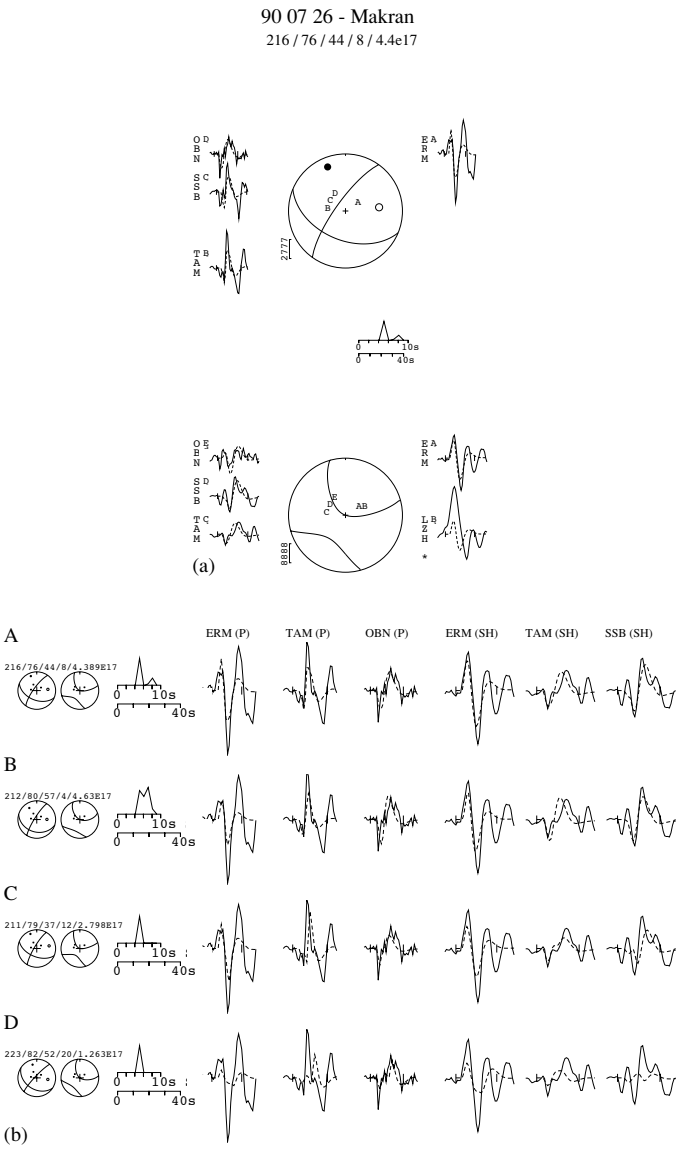

Figure A13. Makran, 1990 July 26. (a) Minimum-misfit solution: strike 216°, dip 76°, rake 44°, depth 8 km, M_w5.7. The *SH* record at LZH (indicated by *) was not used in the inversion. (b) Sensitivity analysis. A: minimum-misfit solution shown in (a). B: depth fixed at 4 km; the synthetics are too narrow at OBN (*P*) and TAM (*SH*). C: depth fixed at 12 km; the synthetics are too broad at TAM (*P*) and SSB (*SH*). Event depth: 8 ± 4 km. D: depth fixed at the EHB value (20 km); the synthetic peak is too late at TAM (*P*) and the amplitudes of the synthetics are too small at most stations.

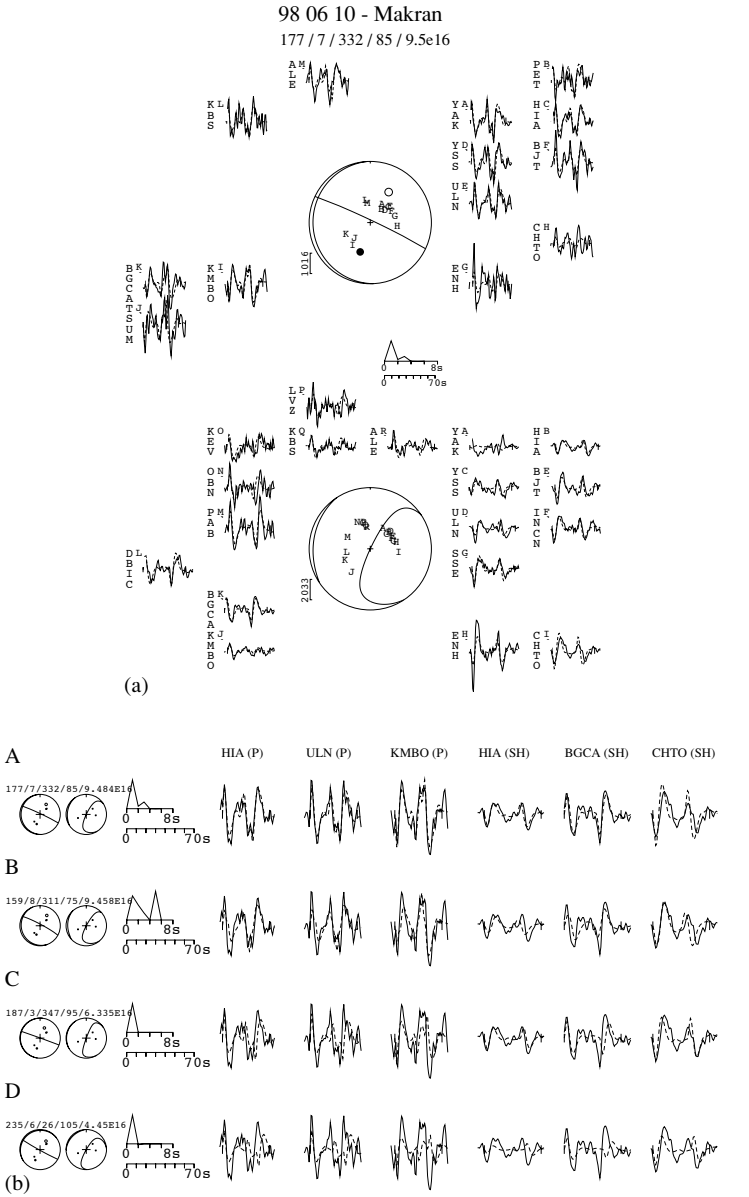

Figure A14. Makran, 1998 June 10. (a) Minimum-misfit solution: strike 177°, dip 7°, rake 332°, depth 85 km, M_w5.3. (b) Sensitivity analysis. A: minimum-misfit solution shown in (a). B: depth fixed at 75 km; the source time function has two peaks. C: depth fixed at 95 km; the synthetic waveforms are too broad. Event depth: 85 ± 10 km. D: the Harvard CMT solution (strike 235°, dip 6°, rake 26°, depth 105 km); the synthetics are too broad to fit the data.

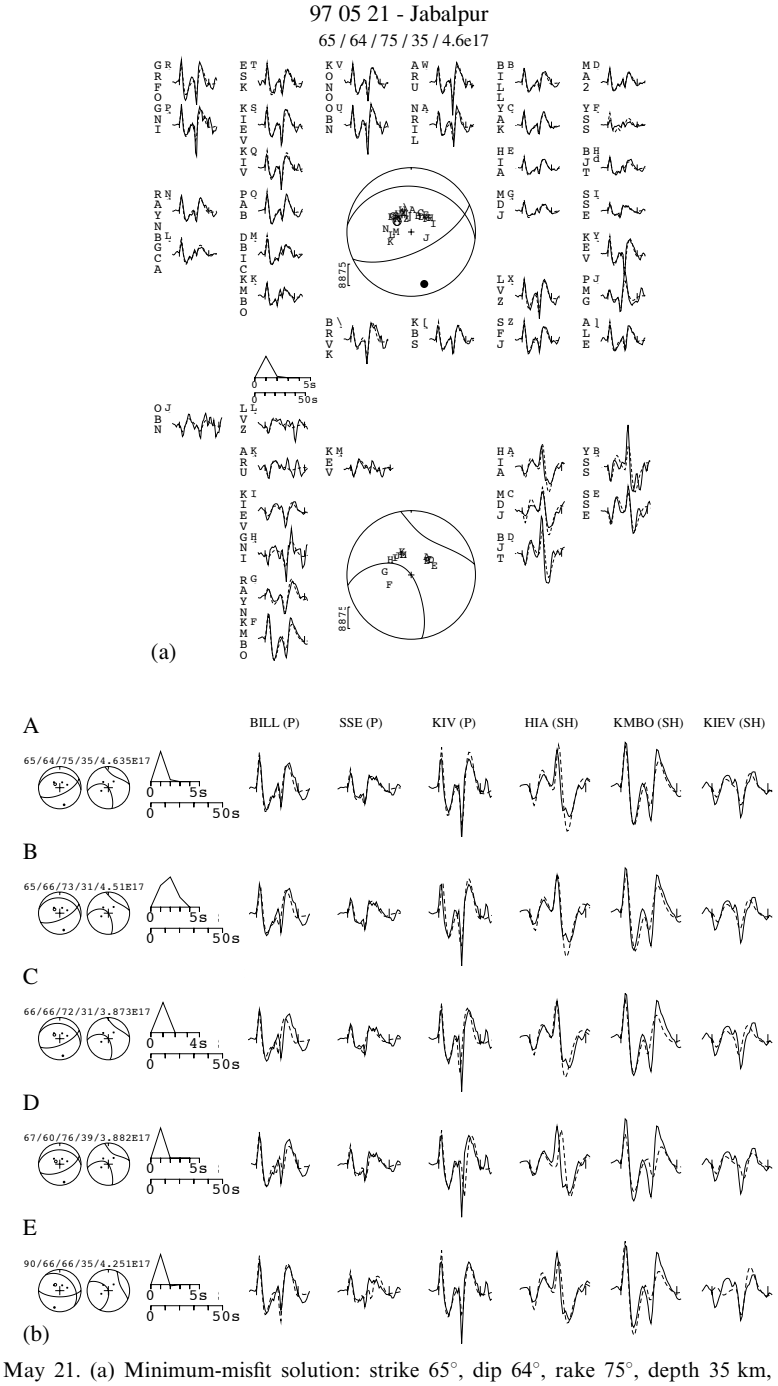

Figure A15. Jabalpur, 1997 May 21. (a) Minimum-misfit solution: strike 65°, dip 64°, rake 75°, depth 35 km, M_w5.7. (b) Sensitivity analysis. A: minimum-misfit solution shown in (a). B: depth fixed at 31 km; the source time function has broadened. C: depth fixed at 31 km, source time function fixed to its value in A; the synthetics are too narrow. D: depth fixed at 39 km; the synthetics are too broad. Event depth: 35 ± 4 km. E: the solution of Battacharya *et al.* (1997), shown for comparison.

bars at either end of the waveform. P and T axes within the sphere are represented by solid and open circles respectively. The source time function (STF) is shown below the P focal sphere, with the waveform timescale below it. (b) The sensitivity analysis, in which each line shows the synthetic waveforms (dashed) generated by the source parameters shown above the focal spheres on the left, and the observed waveforms (solid) at a number of stations. Line A in each plot shows the minimum-misfit solution. Other lines show the effects on the fits of the synthetic waveforms of fixing one or more source parameters at values different from the minimum-misfit ones. A comparison with the Harvard CMT solution is shown, where the depth of the solution lies outside the uncertainties of the minimum-misfit solution; the focal mechanism and depth are set at the Harvard solution, and the moment and source time function shown are those that minimize the misfit to the data.

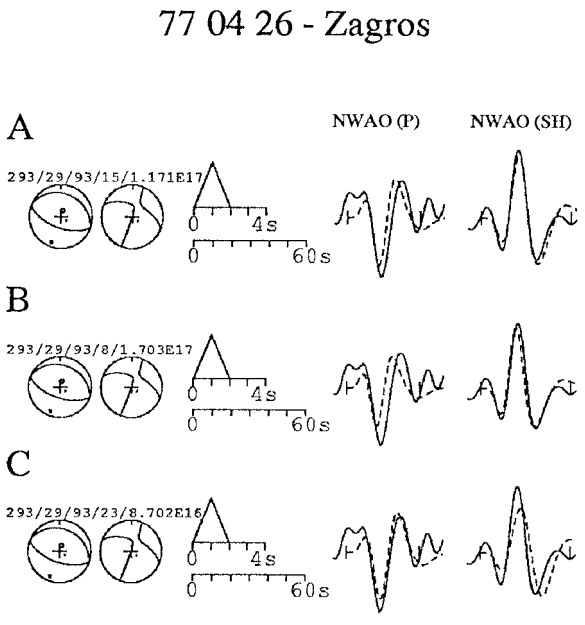

Figure B1. Zagros, 1977 April 26. Good-quality digital records were available only from station NWAO. We used the CMT mechanism (strike 293°, dip 29°, rake 93°) to calculate all the synthetics using MT5. A: best-fit depth: 15 km. B: depth fixed at 8 km; the synthetic pulse is too narrow at NWAO (*P*). C: depth fixed at 23 km; the synthetic pulse is too broad at NWAO (*SH*).

Where the EHB depth is outside the uncertainties of the minimum-misfit solution, we add a line that shows the best possible fit to the data with the depth fixed at the EHB value.

APPENDIX B: FORWARD MODELLING FOR DEPTH ONLY

This appendix contains the depth modelling results (Figs B1–B6) for the six 'b' class earthquakes in Table 1 that are not already discussed in the text. Where more than two broad-band records or only long-period records were available, we used the program MT5 (McCaffrey & Abers 1988) to generate synthetic seismograms with the WWSSN long-period response as described in Section 2.1. For these events, the figures show the fit of the synthetics (dashed lines) to the data (solid lines) at a series of depths; the first line shows the best-fit depth at either the Harvard CMT or the best-fit focal mechanism. In the other cases (Figs B2 and B6) we used the program WKBJ3 (Chapman *et al.* 1978) to generate synthetic seismograms with the WWSSN short-period response as described in Section 2.2. In these figures the synthetics are shown below the short-period record, starting with the synthetic calculated for the best-fit depth at the Harvard CMT mechanism.

In all figures, comparisons with the Harvard CMT or EHB depths are shown only where these depths lie outside the uncertainties in depth of the waveform-determined solution.

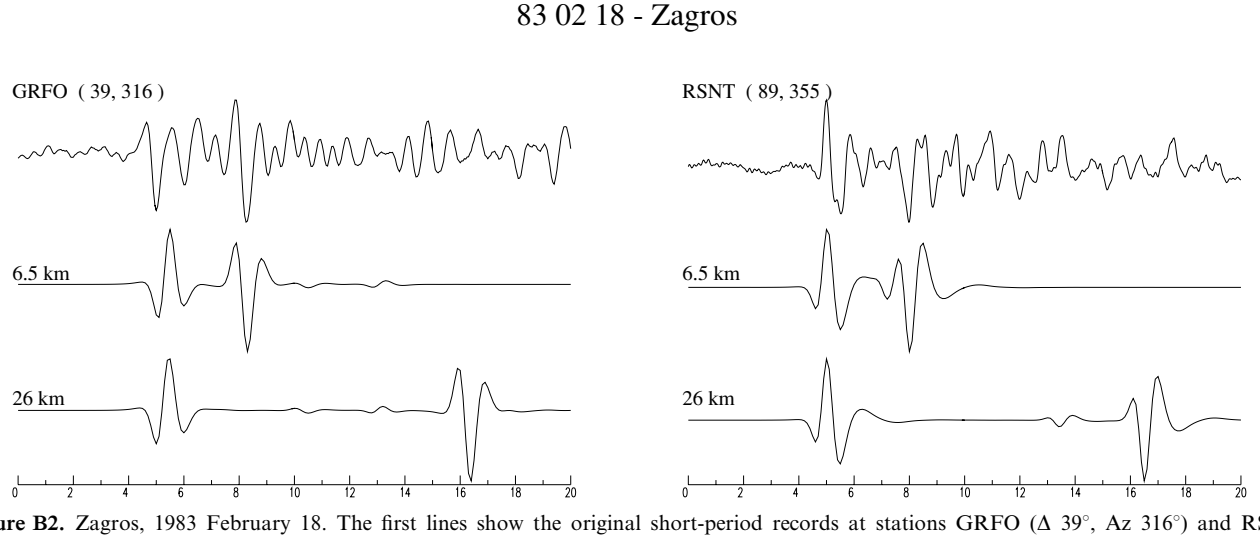

Figure B2. Zagros, 1983 February 18. The first lines show the original short-period records at stations GRFO (Δ 39°, Az 316°) and RSNT (Δ 89°, Az 355°). Synthetics were calculated with WKBJ3 using the CMT focal mechanism (strike 272°, dip 20°, rake 94°). We show synthetics for our best-fit depth (6.5 km) and the EHB depth (26 km).

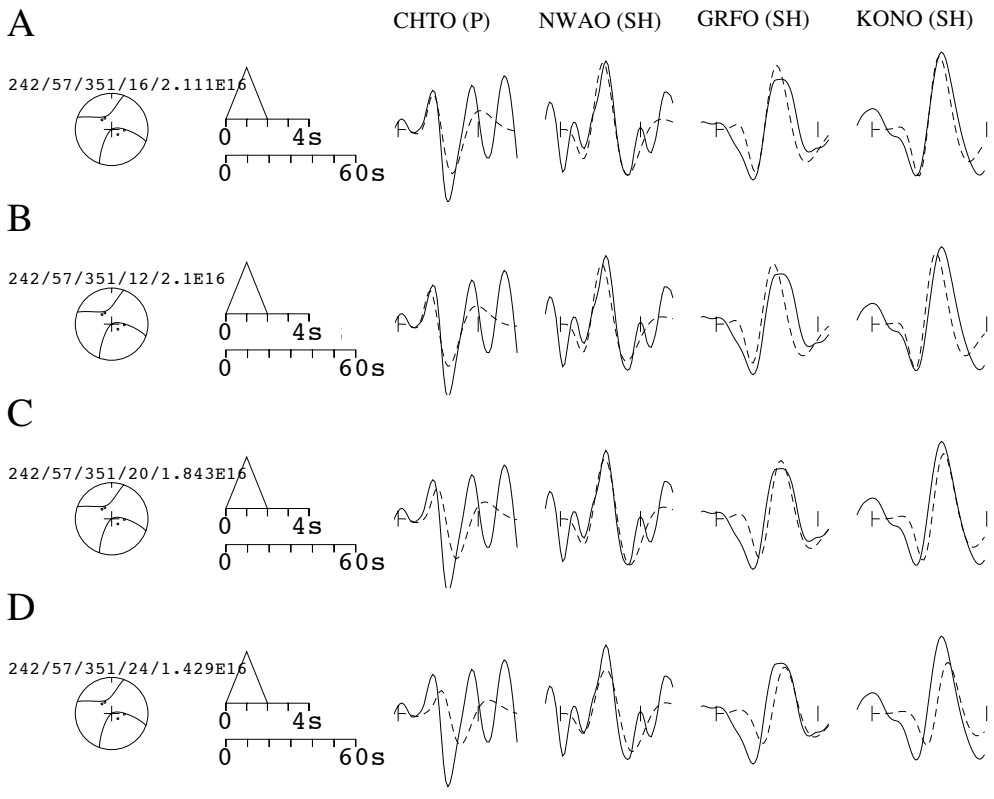

Figure B3. Zagros, 1988 August 30. Only *SH* waveforms had large enough signal-to-noise ratios to be used. All synthetics were calculated with the Harvard CMT focal mechanism (strike 242°, dip 57°, rake 351°) using MT5. A: best-fit depth: 16 km. B: depth fixed at 12 km; the synthetics are too narrow at NWAO, GRFO and KONO. C: depth fixed at 20 km; the synthetics are too broad at CHTO, GRFO and KONO. Event depth: 16 ± 4 km. D: depth fixed at the EHB depth (24 km); the synthetics are too broad at all stations.

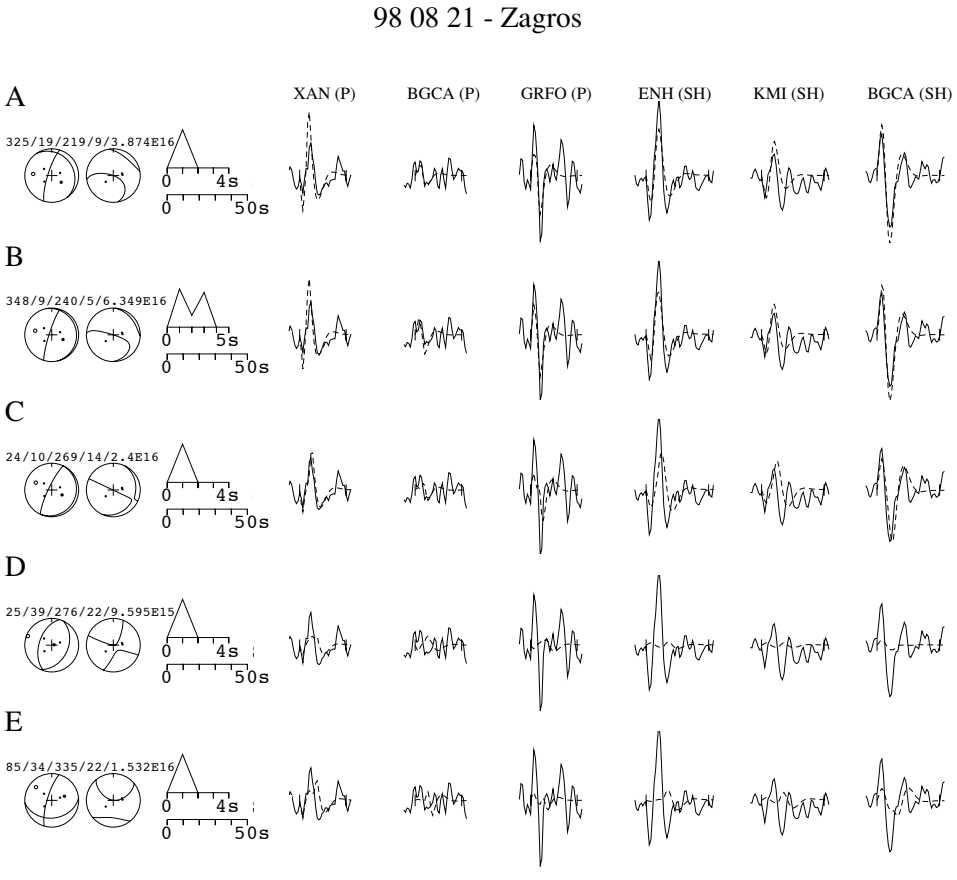

Figure B4. Zagros, 1998 August 21. Synthetics were calculated using MT5. A: best-fit solution: depth 9 km. B: minimum-misfit solution for a depth of 5 km; the source time function has two peaks. C: minimum-misfit solution for a depth of 14 km; the synthetics are too broad at ENH (*SH*) and KMI (*SH*). Event depth: 9^{+5}_{-4} km. D: the Harvard CMT solution (strike 25°, dip 39°, rake 276°, depth 22 km); the nodal planes pass close to stations with non-nodal waveforms. E: minimum-misfit solution for the EHB depth (22 km); the synthetic pulse is too broad at XAN (*P*) and BGCA (*P*), and the amplitudes are too small at the other stations.

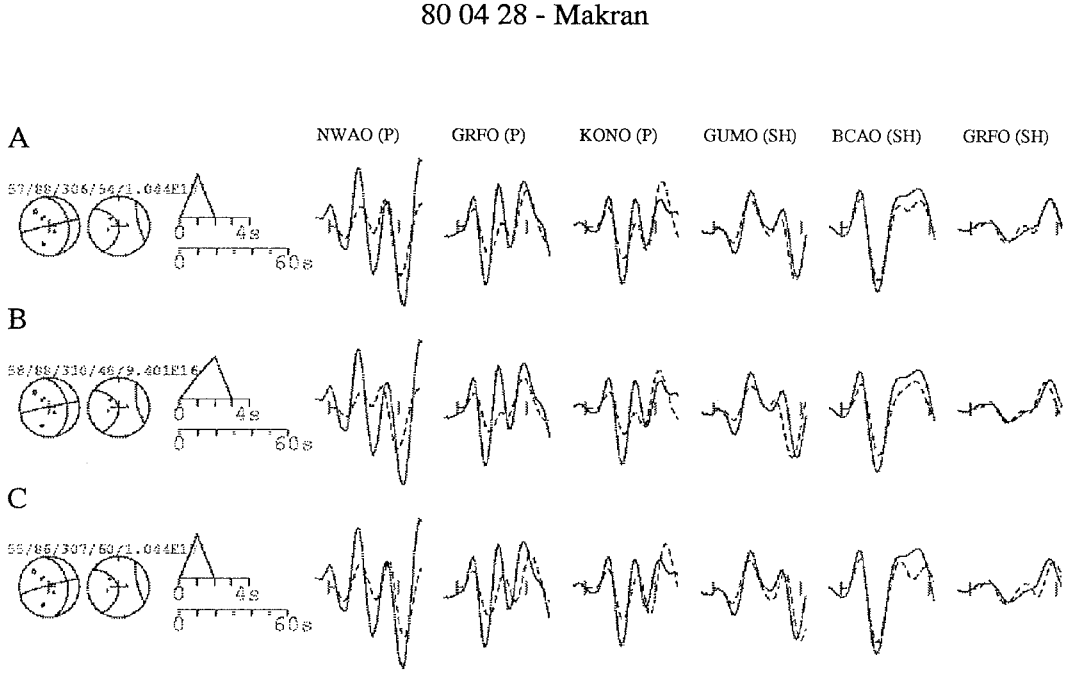

Figure B5. Makran, 1980 August 28. Synthetics calculated using MT5. A: best-fit solution: depth 54 km. B: minimum-misfit solution for a depth of 48 km; the synthetic pulse is too narrow at GUMO (*SH*) and GRFO (*SH*). C: minimum-misfit solution for a depth of 60 km; the synthetic pulse is too broad at GRFO (*P*), GUMO (*SH*) and GRFO (*SH*). Event depth 54 ± 6 km.

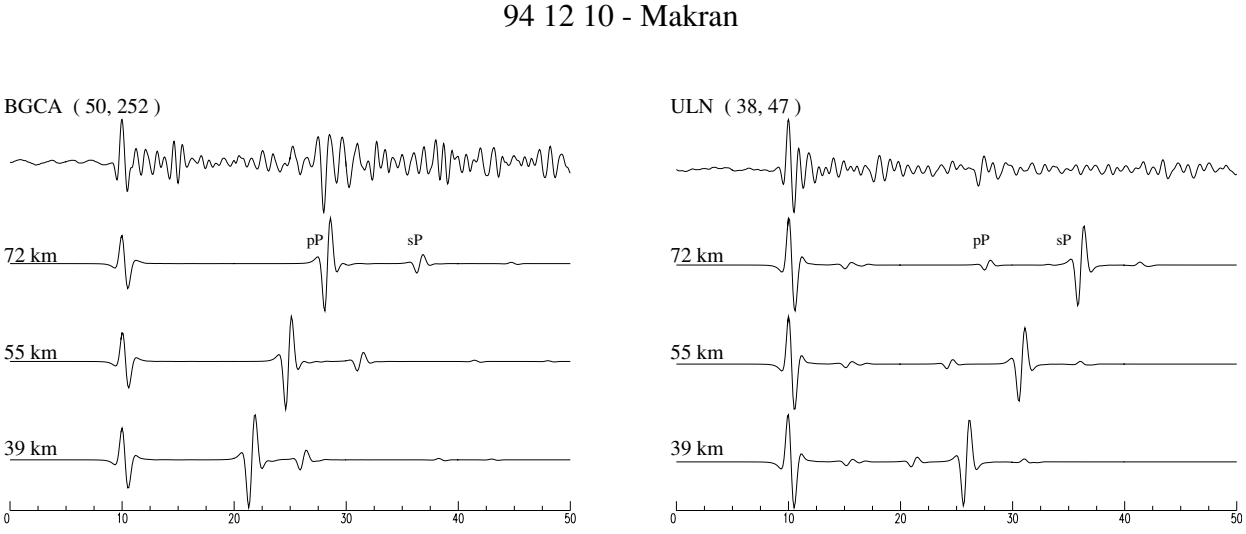

Figure B6. Makran, 1994 December 10. The first lines show WWSSN short-period records at stations GRFO (Δ 39°, Az 316°) and RSNT (Δ 89°, Az 355°). Synthetics were calculated with WKBJ3 using the CMT focal mechanism (strike 204°, dip 37°, rake −130°). We show synthetics for our best-fit depth (72 km), the EHB depth (55 km) and the Harvard CMT depth (39 km).